HHS Public Access

Author manuscript

J Med Chem. Author manuscript; available in PMC 2017 July 12.

Published in final edited form as:

J Med Chem. 2017 March 09; 60(5): 2099–2118. doi:10.1021/acs.jmedchem.6b01869.

Targeting Bacillosamine Biosynthesis in Bacterial Pathogens: Development of Inhibitors to a Bacterial Amino-Sugar Acetyltransferase from *Campylobacter jejuni*‡

Joris W. De Schutter[1], **James P. Morrison**[1], **Michael J. Morrison**[1], **Alessio Ciulli**[2], and **Barbara Imperiali**[1,3,*]

[1]Department of Chemistry, Massachusetts Institute of Technology, 77 Massachusetts Ave., Cambridge, MA 02139, USA [2]Division of Biological Chemistry and Drug Discovery, School of Life Sciences, University of Dundee, Dundee, Scotland [3]Department of Biology, Massachusetts Institute of Technology, 77 Massachusetts Ave., Cambridge, MA 02139, USA

Abstract

The glycoproteins of selected microbial pathogens often include highly modified carbohydrates such as 2,4-diacetamidobacillosamine (diNAcBac). These glycoconjugates are involved in host cell interactions and may be associated with the virulence of medically-significant Gram-negative bacteria. In light of genetic studies demonstrating the attenuated virulence of bacterial strains in which modified carbohydrate biosynthesis enzymes have been knocked out, we are developing small molecule inhibitors of selected enzymes as tools to evaluate whether such compounds modulate virulence.

We performed fragment-based and high-throughput screens against an amino-sugar acetyltransferase enzyme, PglD, involved in biosynthesis of UDP-diNAcBac in *C. jejuni*. Herein we report optimization of the hits into potent small molecule inhibitors (IC_{50} <300 nM). Biophysical characterization shows that the best inhibitors are competitive with acetyl coenzyme A and an X-ray co-crystal structure reveals that binding is biased towards occupation of the adenine sub-pocket of the AcCoA binding site by an aromatic ring.

Graphical Abstract

‡This paper is dedicated to the memory of Austin L. Travis

*To whom correspondence should be addressed: Phone: +1-617-253-1838, imper@mit.edu.

Supporting Information

Supporting information accompanying this paper includes NMR spectra and LC-MS chromatograms of selected inhibitors, molecular formula strings table, enzyme inhibition studies, DLS studies, and X-ray crystallography data.

PDB IDs: 5T2Y and 5TYH The atomic coordinates and experimental data will be released on the PDB upon article publication.

Author Contributions

J.P.M., M.J.M. and A.C. were involved in the initial stages of the project, including enzyme expression and assay development, fragment screening and determination of the 5TYH structure, MLPCN screening and thienopyrimidinone hit validation. J.W.D. S. synthesized the thienopyrimidine series compounds, carried out biochemical and biophysical assays and determined the 5T2Y structure. J.W.D. S. and B.I. wrote the paper and all authors contributed to editing the final manuscript.

Conflict of interests

The authors declare that there is no conflict of interests

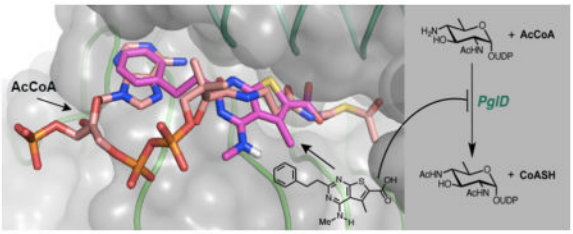

Introduction

Most clinically relevant antibiotics are targeted at essential bacterial survival functions including replication, transcription, translation, and cell wall biosynthesis.[1] This is an outcome of *in vitro* antibiotic screening and discovery, which has relied on observing cell death in culture in laboratory settings. The emergence of resistance against all major mechanisms of antibiotic action requires new paradigms for combating infectious disease. A potentially promising approach includes the development of agents that target bacterial virulence *in vivo* in human hosts. Such approaches may mitigate the effects of infectious disease, while potentially resulting in less selective pressure for resistance development.[2] Virulence factors are implicated in many bacterial processes including host-cell adhesion, invasion, and colonization, as well as quorum sensing and biofilm formation.[2–5] In order to develop antivirulence agents, it is critical to identify validated pathogen-specific processes that cause virulence in the targeted human hosts.

Protein glycosylation is widespread in nature and regulates a variety of cellular functions including protein folding, cell-cell interactions, cell signaling, and the host immune response.[6] Glycans are attached to proteins via either serine/threonine (O-linked) or the amide nitrogen of asparagine (N-linked). It is now recognized that selected bacteria possess the biosynthetic machinery for O- and/or N-glycosylation and that this modification may play a role in pathogenicity.[7–11] N-glycosylation was first discovered in *C. jejuni* in 1999 and the protein glycosylation (pgl) pathway has been characterized in detail for this organism (Figure 1).[12,13] In *C. jejuni*, more than 60 proteins, including confirmed virulence factors, are modified with a conserved heptasaccharide.[14]

In a significant divergence between prokaryotes and eukaryotes, bacteria and archaea have specialized enzymatic processes to modify the structures of selected carbohydrates for incorporation into glycoconjugates. Furthermore, the discovery of unique prokaryote-specific sugars is continuing with the pace of bacterial genome sequencing and bioanalytical methods development.[7] In contrast to the glycosyltransferase enzymes, which assemble complex glycans and share common folds and mechanisms across domains of life, the specialized sugar-modifying enzymes are attractive targets for developing targeted antivirulence agents because they tend not to have mammalian homologs and because the associated glycoconjugates are linked with bacterial pathogenicity.[15] Of particular interest is di-N-acetylbacillosamine (diNAcBac),[16] which is derived from N-acetylglucosamine (GlcNAc). DiNAcBac is found, for example, at the reducing end of O-linked glycans in selected strains of *N. gonorrhoeae* and *A. baumannii*, and N-linked glycans in *C. jejuni*, highlighting the importance of diNAcBac biosynthesis pathways in these Gram-negative

pathogens.[17] Intriguingly, while protein glycosylation pathways from these pathogens glycosylate diverse proteins with different glycans, the reducing-end sugar is diNAcBac.[18–20] The N-linked protein glycosylation (pgl) pathway of *C. jejuni* and steps leading to diNAcBac biosynthesis are illustrated in Figure 1. The first two steps of UDP-diNAcBac biosynthesis utilize an NAD^+-dependent dehydratase (PglF) followed by a pyridoxal phosphate-dependent aminotransferase (PglE) to produce a UDP-4-amino-sugar, which is then acetylated by PglD using acetyl coenzyme A (AcCoA) as a co-substrate (Figure 1 inset).[18] Subsequent glycan assembly onto an undecaprenyl-diphosphate carrier, is catalyzed by a series of glycosyl transferases. After assembly, the completed heptasaccharide is translocated across the inner membrane and the glycan is transferred to protein substrates in the bacterial periplasm by the oligosaccharyl transferase PglB.

Studies have shown that disruption of genes responsible for diNAcBac biosynthesis (*pglF*, *pglE*, *pglD*) perturb production of the native heptasaccharide glycosyl donor in *C. jejuni*.[21] In addition, *ΔpglD* and *ΔpglE* strains show greatly reduced colonization of the gastrointestinal tract of 1-day-old chicks, thereby establishing a link between protein N-glycosylation and *C. jejuni* pathogenicity in host cells.[22] Further insight into these effects came from transposon mutagenesis experiments, which identified *pglF* and *pglE* as essential genes for colonization. In mice, mutation of *pglE* impaired invasion of intestinal epithelial cells and colonization of the gut.[23] The causative glycoconjugates underpinning these findings remain unknown, but several molecular associations between N-glycosylation and *C. jejuni* virulence have been defined. For example, VirB10, a structural component to the type IV secretion system (TFSS), needs to be glycosylated at Asn97, otherwise a 10-fold decrease in natural competency results.[24] Recently, 16 N-linked glycoproteins were identified and found to be associated with *C. jejuni* outer membrane vesicles (OMVs) including the PEB3 adhesin.[25] Pathogens deploy OMVs to deliver bacterial proteins into host cells, making this an important finding in the relationship between periplasmic glycoproteins and virulence.[26] Protein O-glycosylation is also associated with virulence; for example, loss of glycosylation of PilE, a constituent of the type IV pilin in *N. gonorrhoeae*, leads to a significant decrease in epithelial cell adhesion.[27]

Herein we report the development of inhibitors targeting the *C. jejuni* PglD, a UDP-amino-sugar acetyltransferase, which catalyzes the third step in diNAcBac biosynthesis. PglD represents an attractive target for inhibitor development as it is well understood from a structural and mechanistic perspective.[28,29] Additionally, PglD is a soluble, well-expressed enzyme, which makes it tractable for structure/activity-driven inhibitor discovery. Crystallographic analysis of PglD reveals a homotrimeric structure with three equivalent active sites formed at the interfaces between adjacent protomers.[28,29] Like many other bacterial UDP-amino-sugar acetyltransferases, PglD is a member of the left-handed β-helix family comprising two domains (Figure 2a); a N-terminal domain with a β-α-β-α-β-α Rossmann fold motif that binds the UDP-4-amino-sugar, and a C-terminal hexapeptide repeat motif that defines the left-handed β-helix that contributes to the AcCoA binding site. PglD has been co-crystallized in the presence of the AcCoA and UDP-4-amino-sugar substrates (Figure 2b).[28] The structural features of PglD and related homologs differentiate these prokaryotic AcCoA-dependent acetyltransferases from their mammalian counterparts,

including for example HAT1 of the GCN5-related N-acetyltransferase (GNAT) superfamily.[30]

Currently, many questions remain as to why modified carbohydrates, such as diNAcBac, are incorporated into bacterial glycoconjugates. Therefore, chemical tools such as small molecule inhibitors that selectively block diNAcBac biosynthesis would be valuable agents for understanding the significance of glycan diversification in selected bacteria. In addition, such tools could help to validate the pgl pathway enzymes as potential antivirulence targets. Consequently, we have established a program to develop inhibitors of diNAcBac biosynthesis with a focus on the well-characterized *C. jejuni* pathway. This Gram-negative pathogen is a common cause of gastroenteritis in humans and may also result in the development of Guillain-Barré syndrome, an auto-immune disease in which the peripheral nerves are attacked resulting in damage to the myelin insulation.[31,32] In recent years, *C. jejuni* has shown increased resistance towards front-line antibiotics including the macrolides and fluoroquinolones, which inhibit protein synthesis and DNA unwinding, respectively.[33]

Results

Screening

Initial hits for the development of inhibitors for PglD were identified by employing fragment-based screening and high-throughput molecular library approaches.[34] The fragment-based screen was performed with a fragment set that included a selection of the Maybridge Ro3 chemical library as described previously.[35] The primary screen involved differential scanning fluorimetry (DSF) analysis against PglD to identify fragments that bind to and stabilize the natively-folded protein. Following this, hits were confirmed by NMR spectroscopy (WaterLOGSY and STD) and further validated using a UV-based biochemical assay, which measures CoASH release following acetyl transfer to the UDP-4-amino-sugar.[36] Using this workflow, 10 compound hits with IC_{50} values in the 1–10 mM range and ligand efficiencies in the 0.29 – 0.32 range were validated. For example, compound **1** (Figure 2), which was analyzed by X-ray in complex with PglD, binds to the central AcCoA binding groove occupying the pantetheine site proximal to active-site residues involved in amino-sugar activation and thioester attack (Figure 2c). Unfortunately, efforts to build upon this, and other validated fragments yielded only modest improvements in affinity. Coincident with these studies a high-throughput screen was performed in collaboration with the Broad Institute, using a Diversity-Orientated Synthesis (DOS) compound collection (83,000) and the NIH Molecular Libraries Probe Production Centers Network (MLPCN) library (276,000) of small molecules.[37] Compounds were screened at 10 μM using a PglD end-point assay monitoring the generation of CoASH from the acetyltransferase reaction. Despite the low hit rate (defined as >20% inhibition) of 0.02% and 0.12% respectively, the screen led to the discovery of thienopyrimidinone-6-carboxylate compound **2** as a promising hit for further development. For direct comparison with the validated fragment hits, **2** was deconstructed to the core structure **3**, which demonstrated a validated IC_{50} value of 860 μM and LE of 0.31. In light of these results and the tractability of the core towards synthetic manipulation at four points of diversification (C2, C4, C5, and C6; Scheme 1) this compound class became the focus of our continuing medicinal chemistry efforts.

Preliminary structure activity studies to vary substitution at C2 generated analog **4** as the best inhibitor with an IC_{50} value of 1 μM (LE 0.33). However, although this compound represented a good improvement in potency, the candidate suffered from some disadvantages. Specifically, **4** features a planar structure with poor solubility properties and a metabolic liability due to the 1,3-unsubsituted indole and conjugated alkene systems. Furthermore, **4** and related analogs showed poor long-term stability in solution. A significant effort was also made to crystallize PglD with several of the thienopyrimidinone hits, however, this proved unsuccessful. Therefore, we performed a docking study on fragment **3** to generate a computational model as a guide for future synthetic efforts aimed at eliminating the compound liabilities while improving potency.[38] The thienopyrimidone-6-carboxylate core was predicted to occupy a binding site overlapping with the panthetheine moiety of AcCoA, as had been previously observed in the co-crystal structure of fragment **1** (PDB 5TYH), with similar placement of the carboxylate moiety and close agreement between the positions of the furan oxygen of **1** and exocyclic oxygen of **2** (compare Figure 2c and d). Given these observations, we exploited the computational model as a guide for the design of the next generation of analogs, which recognized the opportunity to extend the molecule *both* at the C2 position to interact with a hydrophobic region on the β-helix, and at the C4 position, by transitioning to the thienopyrimidine core, to further occupy the AcCoA binding groove (Scheme 1).

In order to reach cytoplasmic targets in Gram-negative pathogens, compounds may enter cells through passive diffusion or pass through the bacterial porins to reach the periplasm and then reach the cytoplasm *via* passive or active mechanisms.[39,40] With these parameters in mind, our overall goal was to develop potent (IC_{50} <500 nM) inhibitors of *C. jejuni* PglD based on the thienopyrimidine-6-carboxylate core with good ligand efficiency (LE >0.30) together with balanced physicochemical properties including cLogP values between 2 – 4.[41]

Chemistry

We developed modular synthetic routes to provide access to the target thienopyrimidine carboxylic acids with readily-modifiable substitution at the C2 and C4 positions (Schemes 2 and 3).

For modification at the C2-position (Scheme 2, Route I), the synthesis was initiated by condensation of commercially available thiophene, **5**, with nitriles bearing the desired R_2 substituent, under strongly acidic conditions. In most cases, the thienopyrimidone products of general structure **6**, proved highly insoluble, and therefore chromatography and NMR characterization was carried out after the subsequent step. In cases where nitriles with the appropriate R_2 moiety were inaccessible, an alternative approach (Route II) was employed. This route is somewhat longer and includes a Michaelis-Arbuzov reaction with triethyl phosphite and analog **6** (Core structure: R_2 = -CH_2Cl) to furnish phosphonate **8**. Subsequent Horner-Wadsworth-Emmons (HWE) olefination and hydrogenation generated thienopyrimidinones of general structure **9** with a variety of phenylethyl substituents at the C2-position.

Installation of a substituent at the C4-position of thienopyrimidines is typically accomplished by transforming the C4 oxygen of the thienopyrimidone into chloride or

bromide, with $POCl_3$ and PBr_3 respectively, followed by a S_NAr reaction, both performed at high temperatures. To avoid use of these harsh conditions and strong lachrymators, we instead employed a one-step, room temperature reaction modified from chemistry developed by researchers at Wyeth.[42] Utilization of a sufficiently strong base, such as 1,8-diazabicyclo[5.4.0]undec-7-ene (DBU), in excess solubilized the thienopyrimidinones in acetonitrile and replacing the toxic and expensive BOP reagent for the readily available PyBOP, allowed for robust formation of the desired pyrimidines of general structure **10** in good yields (40–90%). These thienopyrimidines could be isolated by column chromatography in excellent purity (>95% homogeneity as determined by LC-MS). The final saponification of thioenopyrimidine esters represented by **7** and **10** was achieved in a THF/MeOH/H_2O mixture containing NaOH; occasionally mild heating was required to achieve complete conversion. The final inhibitors with core scaffold **11** were isolated by trituration as easy to handle solids.

A related thienopyrimidine isomer with general structure **16**, was accessed as described in Scheme 3. In this case, the thiophene starting material **14** is not commercially available but could be readily prepared by the esterification of dicarboxylic acid **12** followed by nitration and hydrogenation. Condensation with nitriles provided thienopyrimidinones of general structure **15**, which differ from the scaffold **11** series in the relative location of the sulfur atom and the absence of a methyl group on the thiophene ring. Installation of substituents at C4 and saponification were performed as described previously, to provide inhibitors with core scaffold **16**.

Initial SAR analysis

All target thienopyrimidine carboxylic acids **11** and **16** (Figure 3) were assayed for inhibition of recombinantly-expressed and purified *C. jejuni* NCTC 11168 PglD acetyltransferase.[18] The continuous assay monitors the release of CoASH using 5,5′-dithiobis-(2-nitrobenzoic acid,[36] and was carried out at 300 μM AcCoA (K_m of 295 μM), and 500 μM UDP-4-amino-sugar (K_m of 274 μM). IC_{50} values of selected compounds are summarized in Table 1. The AcCoA concentration was aligned with reported physiologic concentrations in typical Gram-negative bacteria.[43]

Our initial strategy was to explore the C2- and C4-substituents individually and then combine the optimal structural components from each series to capture advantageous synergistic binding effects. We observed that short aliphatic chains and saturated carbocycles at C2 (with R_4 = Me) provided weak inhibitors with IC_{50} values in the 10 μM to 1 mM range (data not shown). Based on these studies we selected an unsubstituted phenylethyl moiety (Figure 3, substituent **d**) as a favorable C2-substituent in terms of potency gain *versus* added mass (e.g. **17**, IC_{50} = 2.2 μM, LE 0.35, Table 1). However, when we explored C4-substituents (with R_2 = H), these analogs proved to be poor inhibitors (IC_{50} > 500 μM, data not shown) and SAR trends could not be well defined from the data. Accordingly, we elected to directly prepare disubstituted analogs, with R_2 = phenylethyl (**d**), and iteratively build up the R_4 substituent in terms of length, sterics and heteroatom substitution (e.g. inhibitors **18**–**35**; shorter and smaller substituents omitted for brevity). In general, only modest gains in potency could be achieved, and all the gains were at the cost of poorer ligand efficiencies.

Ultimately, we observed that a phenylethyl moiety was also well tolerated at the C4-position of the thienopyrimidine core (**20**, $R_2 = R_4$ = phenylethyl, IC_{50} = 1.4 μM).

In order to gain a better understanding of the binding behaviour of the inhibitors, we examined the results of the phenyl scan on the R_4 substituent, which positioned moieties with different characteristics (sterics, polarity and hydrogen-bonding capabilities) *ortho*, *meta* or *para* on the aryl ring (inhibitors **21**–**35**). However, while we had predicted that these substitutions would either complement or clash with the protein surface resulting in a measurable difference in IC_{50} values, we instead observed a "flat" SAR with inhibitors exhibiting IC_{50} values around 0.5 μM (e.g. **21**–**35**). Indeed, only substitution with an acetamido group (**33**–**35)** elicited clear variances, with the *ortho* substitution being the most disfavored (**35**, IC_{50} = 9.0 μM). A potential explanation for the flat SAR could be that if the aryl group occupies the AcCoA binding groove then one edge would face the protein surface and the other would be solvent exposed, thus precluding any interaction between the moieties on the R_4-aryl ring and the protein surface. This hypothesis was tested by preparing analogs bearing two moieties on the aryl ring (inhibitors **36**–**38**), however, potency remained at 0.5 μM.

In light of these data, we developed two hypotheses. One potential hypothesis was that the compounds might have a different mode of action other than competitive inhibition with the AcCoA substrate. We explored this by applying several biochemical and biophysical approaches, which are presented in the next section (*vide infra*). The second possibility was that the inhibitor binding mode differed significantly from that predicted by the computational model; for example, either the ligands bind in a different location on the PglD protein surface or the enzyme itself undergoes a significant conformational change. We also noted that the C2, C4-disubstituted inhibitors were inherently quite symmetrical, with a pseudo C_2 axis of rotation in the plane of the thienopyrimidine core (Figure 4a). This feature might explain the flat SAR observed for the phenyl scan of the R_4-substituent since the effect of any moiety on the aryl group could potentially be masked if the ligand flipped 180° and positioned the R_2-substituent in the AcCoA binding groove instead. To test this hypothesis, we synthesized inhibitors **49** and **50**, which included the quasi-regioisomeric thienopyrimidine core **16** and, if the binding orientation remains true, should position the sulfur atom towards the protein surface. Indeed, these inhibitors had similar potency to their parent analogs (compare **49** IC_{50} = 3.9 μM vs. **17** IC_{50} = 2.2 μM, and **50** IC_{50} = 1.4 μM vs. **41** IC_{50} = 1.1 μM), suggesting the thienopyrimidine carboxylic core can bind in either of two orientations into the AcCoA binding groove. To further validate this hypothesis, we developed inhibitors that would be locked in a fixed conformation by introducing rigidifying elements in the alkyl linkers between the thienopyrimidine core and substituent aryl groups. Synthetically it was straightforward to add a methyl group on the second carbon of the R_2-substituent and a methoxy group on the second carbon of the R_4-substituent; the prerequisite starting materials were commercially available as both stereoisomers and could be easily transformed into the corresponding nitrile or amine for the modular syntheses (Figure 4b). With the four rigidified analogs we would expect to see data consistent with a matched/mismatched phenomenon; either substituent should have an enantiomer that complements the protein surface better than the other and when combined these effects should result in

one poor inhibitor, two moderate ones and a single preferred analog. Indeed, this was observed with compounds **51**–**54** (Figure 4b), albeit in a modest IC_{50} range. These combined results strongly suggested that the inhibitors were capable of binding to the PglD active site with either the R_2-, or R_4-substituent in the AcCoA groove.

Overall, the SAR data (Figure 4) shows that while binding may be somewhat promiscuous, the R_2-substituent was far more important for binding potency. This experimental observation was therefore inconsistent with our initial computational model, which had oriented this substituent over the β-helix (and quite solvent exposed) and placed the R_4-substituent in the AcCoA groove. These findings prompted us to investigate the binding mode in more detail, to provide a foundation for the next synthetic and biochemical efforts.

Biophysical characterization and inhibitor optimization

With the knowledge gained from SAR studies up to this point, we generated a potent *C. jejuni* PglD inhibitor, **55** (Figure 5), with an IC_{50} of 270 nM; however, this was at the cost of decreased ligand efficiency (0.26) and a high cLogP (5.12). In order to further optimize the potency and physicochemical properties of these compounds, we needed to better characterize their binding characteristics. Towards this end, we employed several complementary approaches including the PglD inhibition assay with varying substrate concentrations, DSF analysis, dynamic light scattering (DLS) and X-ray crystallography.

We had first initiated inhibitor development based on modeling studies, which suggested that the thienopyrimidine carboxylate core competed with the AcCoA substrate for binding to the PglD active site. To test this experimentally, we monitored inhibition in the presence of varying concentrations of the two substrates. We observed that significantly higher concentrations of the UDP-4-amino-sugar substrate had no measurable effect on the inhibition by a representative analog of **11** (compound **37**, supporting information Table S2). In contrast, a 2-, and 5-fold increase in AcCoA substrate concentration resulted in measured IC_{50} values of 0.63 μM and 1.4 μM, respectively. These values represent a 2- and 4-fold decrease in potency and strongly suggest that the thienopyrimidine carboxylate inhibitors compete with AcCoA for binding to the PglD active site.

All of the data thus far has been based on the enzymatic inhibition assay and, despite the judicious use of detergent and BSA to prevent aggregation phenomena,[44] may be prone to artefacts that obscure binding trends. We therefore employed DSF as a qualitative secondary assay to assess binding of inhibitors to the *C. jejuni* PglD. DSF employs a fluorescent dye, Sypro Orange, to report on the thermal denaturation of a protein or protein/ligand complex.[45] Potent inhibitors bind to their target enzyme more strongly that weak ones, resulting in a more stable protein/ligand complex and higher measured melting temperature (T_m). Therefore, the thermal stabilization (ΔT_m) of PglD can be used to provide an indirect measure of the *relative* binding affinity of the *related* family of compounds. We selected a subset of inhibitors with a range of IC_{50} values and structural characteristics to analyze by DSF and plotted the ΔT_m *vs* IC_{50} values (Figure 6). The graph shows a positive correlation ($R^2 = 0.72$) between inhibition potency and thermal stabilization over a range of IC_{50} values indicating that the compounds stabilize the native PglD homotrimer and that the more potent compounds, based on IC_{50} values, indeed stabilize PglD more effectively.

Next, we analyzed the enzyme quaternary structure in solution by dynamic light scattering (DLS) and found the calculated hydrodynamic radius of apo PglD to be ~34 Å, consistent with the crystal structures of trimeric PglD (supporting information Figure S1). In the presence of 10-fold excess of inhibitor **55**, the measured radius was marginally larger, ~36 Å, yet still consistent with the known trimeric structure. We also noted that the polydispersity index (PDI) of the PglD/**55** complex (24 % PDI) was lower than apo PglD (31% PDI), providing strong support that the inhibitor does not destabilize quaternary structure and indeed binds to the homotrimeric enzyme.

Throughout these efforts we also continued to pursue crystallization attempts to gain structural insight on representative thienopyrimidine analogs. X-ray analysis of the *C. jejuni* NCTC 11168 PglD enzyme has been successfully carried out in our group and others.[28,29] Typically, the reported precipitant solutions were either high ionic strength (1.9 M ammonium sulfate) or contained acidic buffer components that were frequently observed to bind in the enzyme active site (sulfate, phosphate, citrate).[28,29] Despite numerous attempts, application of previously published protocols did not yield co-crystal structures with the current thienopyrimidine-6-carboxylate inhibitors and thus we screened for new conditions that would be more compatible with the binding of small organic molecules. Ultimately, a crystallization hit with PEG-3350 was successfully optimized to reliably produce high quality crystals. The crystals develop as hollow, hexagonal rods that fill in from one end as they mature; producing either “vase-like” or solid crystals (Figure S3). The diffraction quality did not appear to differ between a solid or hollow end of such crystals. The crystals were tolerant of DMSO in concentrations up to 10%, but tended to be rather fragile and could break upon looping. Therefore, we employed an “in-drop soaking” protocol, in which a solution of the inhibitor is directly added to the drop containing the crystals.

Using these crystallization conditions, we were able to obtain high-quality diffraction data and successfully solve the co-crystal structure of the PglD/**17** complex (Figure 7 and S4). From the structure, two significant observations were immediately evident. Firstly, as anticipated from the SAR studies, the thienopyrimidine core was flipped 180° compared to the computational model developed with the core fragment, with the R_2-subsituent binding in the AcCoA groove (Figure 7, panel b). This position of the thienopyrimidine core directs the R_4-subsituent away from the AcCoA groove and into solvent where it makes no significant interactions with the PglD protein surface (Figure S5, LigPlot[46]). This observation is consistent with our SAR findings that R_4-subsituent makes small contributions to inhibitor potency at the expense of ligand efficiency (Table 1). Secondly, the most surprising observation was that the ligand was bound 3.9 Å further along the AcCoA groove, relocating the carboxylate distal to the acetyltransferase active site where the AcCoA thioester is normally accommodated. This observation was rather unexpected as we assumed that the Asn118, H134 and S136 residues would be preferred hydrogen-bonding partners for the inhibitor carboxylic acid moiety. Furthermore, this displacement precludes a T-shaped **π**-stacking between the side chain of Phe152 and the thienopyrimidine core; instead the binding mode positions Phe152 at an offset angle over the inhibitor carboxylate (Figure S4). To compensate, inhibitor **17** makes several other key interactions with the PglD surface; the carboxylic acid moiety is positioned at a favorable distance and orientation to

form hydrogen bonds with the Ser136 side chain and the backbone amide NH of Ile155. Similarly, the thienopyrimidine N1 atom is well placed to interact with Gly173. From the structure it appears that a definitive interaction may be the placement of the R_2 phenyl ring within the AcCoA adenine binding sub-pocket, displacing solvent waters from a relatively hydrophobic protein cavity. The ligand binding mode is also internally favorable (low torsion) as the bound conformation adopts an anti-periplanar angle of approximately 160° along the benzylidene bond between the thienopyridimine core and R_2 phenyl ring (Figure 7c).

Armed with this new structural information we set out to further optimize the inhibitor series. First we investigated the possibility of simultaneously placing the R_2 phenyl ring in the adenine sub-pocket and the carboxylate in the active site hot spot by increasing the linker length between the inhibitor core and R_2-substituent. This did not prove successful as analogs **39** and **40** (with a 3- and 4-carbon linker respectively) demonstrated lower *in vitro* potency; presumably due to internal strain of unfavorable torsion angles of the alkyl linker. Secondly we noted that although the R_2 phenyl group fits well in the adenine sub-pocket, it does not fully occupy the volume of the [6,5]-fused ring cavity and there was unoccupied space at the *meta* position relative to the linker (Figure 7c). We explored several moieties at this position (**41** –OMe, **42** –F, **46** –Cl and **47** –CF_3, Table 1), but only gained a minor improvement in potency with compound **41** (IC_{50} = 1.1 μM). Finally upon closer inspection of the adenine sub-pocket we speculated that if the aromatic carbon at a position *ortho* to the linker is replaced by a nitrogen and protonated, it would be well-oriented to form a hydrogen bond with the backbone oxygen of Gly173, as it does with the exocyclic amine of the adenine of the AcCoA substrate (PDB ID 3BSY).[28] While the resultant pyridine nitrogen is only weakly basic, it could potentially be protonated in the microenvironment of the enzyme and lead to an order of magnitude improvement in potency. For example, the pyridine derivative risedronic acid is a ~300-fold more potent inhibitor of the human farnesyl pyrophosphate synthase than the corresponding phenyl analog.[47] Although not as significant, the 4.8-fold fold enhancement we observed between inhibitor **43** (IC_{50} = 0.46 μM) and **17** (IC_{50} = 2.2 μM) is very interesting considering the minor nature of the structural change. Although **43** is not the most potent inhibitor, it exhibits the best ligand efficiency, 0.39, and has a cLogP of 2.94, within the −0.5 – 3 range that is thought to be ideal to reach cytoplasmic targets of Gram-negative bacteria; with these characteristics **43** represents our best candidate to date with balanced physicochemical properties.

Discussion and Conclusions

In the development of inhibitors of the *C. jejuni* UDP-4-amino-sugar acetyltransferase, PglD, we initially screened both fragment-based and HTS libraries. These studies led to the identification of a thienopyrimidine-6-carboxylate core as a promising hit. Over the course of the SAR studies we found substitution at the C2-position of the core to be most impactful and that the binding mode appeared to be poorly predicted *in silico*. By combining data from substrate competition assays, DSF, and DLS we confirmed that the inhibitors bind exclusively to the AcCoA binding groove of the active site without disrupting the homo-trimeric structure of PglD.

Critically, crystallographic analysis reveals a 180° flip of the thienopyrimidine core to place the R_2-substituent in the AcCoA groove, as was anticipated from the SAR data. However, in contrast to previously characterized small fragments, we observed a 3.9 Å displacement of the inhibitor further along the AcCoA groove away from the known thioester binding site. Notably, in this new binding mode, the inhibitor makes several hydrogen-bonding interactions that compensate for the ones that would have been formed with the key catalytic residues (Asn118 & His134), but also precludes a stabilizing T-shaped π-interaction between the thienopyrimidine core and Phe152. Ultimately, it appears that placement of the R_2-phenyl into the adenine sub-pocket of AcCoA binding site may be the main driving force of ligand binding and indeed further optimization of this interaction resulted in to our most promising lead. Specifically, inhibitor **43** (IC_{50} = 0.46 μM) shows an excellent ligand efficiency of 0.39 and a favorable clogP of 2.94. To the best of our knowledge this is the first competitive inhibitor with an IC_{50} value < 1 μM for a bacterial amino-sugar-modifying enzyme. A selection of inhibitors from the series presented herein was also tested against the structurally homologous amino-sugar acetyltransferase from *N. gonorrhoeae* (PglC in that O-linked glycosylation pathway) and no significant inhibition was observed even at 100 μM. This observation was not surprising considering the significant differences between the AcCoA binding sites of the two enzymes.[48]

With respect to biological analysis, the *in vivo* analysis of inhibitors that target bacterial virulence factors requires more complex experimental approaches than the simple estimation of minimal inhibitory concentrations (MICs) used in assessing bacterial viability with antibiotics that are targeted at cell survival processes. We are therefore pursuing multiple strategies to investigate *in vivo* efficacy both directly in *C. jejuni*, by assessing the impact of the inhibitors on glycoprotein biosynthesis, and in cell culture models of mammalian gut endothelia assessing *C. jejuni* adhesion and invasion. Currently, despite robust *in vitro* activity, we do not observe a reduction in glycosylation of periplasmic and cell surface proteins upon treatment of *C. jejuni* with the current inhibitors. This observation may be the result of insufficient inhibition potency against the target and/or may result from limited cellular uptake or efflux. In this context, *C. jejuni* features both a formidable cell wall including inner and outer cell membranes flanking a peptidoglycan barrier together with a dense external glycocalyx, as well as an active CmeABC efflux pump system to guard against external chemical agents.[49] With respect to potency, the X-ray analysis of PglD with compound **17** provides an excellent foundation for further structure-guided optimization of the thienopyrimidine core. Concerning cellular uptake and efflux, which are common impediments to antibiotic activity in Gram-negative pathogens, the presented thienopyrimidine core also offers considerable opportunities. In particular, we are exploring several strategies including bioisosteric replacement of the carboxylate moiety and development of pro-drug analogs in consideration of the fact that the negative charge of the carboxylic acid moiety might acting as an impediment for compound uptake into the cytoplasm, which is the site of PglD activity. Additionally, the C4-substituent of the thienopyrimidine series represents a valuable handle for modulating the cLogP of the inhibitor, since we have demonstrated that substitution at this site can be varied without adversely perturbing PglD inhibition. As elegantly demonstrated in a recent study of another Gram-negative pathogen, researchers have shown that fine-tuning the physical properties of

inhibitors, in this case to mimic the zwitterionic charge distribution of amino acids, allowed novel carbapenem analogs to pass through the OccD1 membrane porin of *P. aeruginosa*.[50] Thus the thienopyrimidine compounds in this report are amenable to further such optimizations and current efforts are focused on overcoming the *C. jejuni* defenses to validate PglD as a potential antivirulence target in the biological context of infection.

Overall the studies presented herein support further development of small molecule inhibitors as tools for investigating of the role diNAcBac in bacterial glycosylation and how it relates to pathogenicity. Promising candidates targeting important virulence factors have already been documented, including agents inhibiting pilus assembly in uropathogenic *E. coli*[51] and bacterial motility by inhibiting disulfide formation of periplasmic proteins.[52] Progress has also been made towards modulators of quorum sensing.[53] Closely related to the work in this paper, the Sulea and Logan research groups have reported an inhibitor that targets the pseudaminic acid biosynthetic pathway found in *H. pylori* and *C. jejuni*.[54] The "sialic-acid like" nonulosonate sugar product is required for the glycosylation of structural flagellin proteins and exposure to inhibitors attenuated flagellin production at concentrations of ≥100 μM. The flagella are required for persistent infections of *H. pylori* and this work demonstrates the link between bacterial glycosylation and pathogenicity using chemical tools (as opposed to genetic modification). The most advanced antivirulence work has been accomplished with N-phenyl-4-(3-phenylthioureido)benzenesulfonamide, **56** (LED209), a prodrug agent that covalently inhibits QseC, a receptor involved in signaling between many Gram-negative pathogens and the infected host.[55] Treatment with **56** in a mouse infection model showed prophylactic efficacy against *S. typhimurium* and provided protection against *F. tularensis* both pre- and post-infection. Furthermore, **56** was not toxic at therapeutic doses and did not affect pathogen growth *in vitro*. These promising *in vivo* results are compelling evidence that killing is not necessarily required for treatment of bacterial infection and alternate therapeutic intervention strategies are worth exploring.

In conclusion, herein we disclose the hit-to-lead development of a new series of thienopyrimidine-6-carboxylate inhibitors of the *C. jejuni* PglD UDP-amino-sugar acetyltransferase enzyme, which, upon further optimization could represent valuable chemical tools for unraveling the intricate biological role(s) of highly modified sugars in bacteria and potentially may lead to new agents with targeted antivirulence activity.

Experimental section

General Procedures for Characterization of Compounds

All intermediate compounds were purified by normal phase flash column chromatography on silica gel using a CombiFlash instrument. The homogeneity of all final compounds was confirmed to ≥95% by analytical reverse-phase LC-MS using an Agilent Series 1100 HPLC instrument equipped with a YMC AQ12S03-1003WT C18 column and a Finnigan LCQ Deca electrospray ionization mass spectrometer, using a gradient of 5–95% in 20 min of acetonitrile in water with 0.1% TFA. Each final compound was fully characterized by ^{1}H and ^{13}C NMR and HRMS. Chemical shifts (δ) are reported in ppm relative to the internal deuterated solvent (^{1}H, ^{13}C), unless indicated otherwise. The high-resolution MS spectra of final products were recorded using direct analysis in real time (DART) ionization on a

Bruker Daltonics APEXIV 4.7 Tesla Fourier Transform Ion Cyclotron Resonance Mass Spectrometer (FT-ICR-MS).

General procedure for the formation of thienopyrimidinones – Parent structure 6

A pressure vessel washed charged with aminothiophene (1 equivalent) and nitrile (1–1.2 equivalents) and 4M HCl in dioxane was added via syringe. The pressure vessel was tightly sealed with a Teflon screw cap stopper and the reaction was stirred at 80°C until the reaction was complete, as judged by TLC. The reaction mixture was cooled to room temperature, transferred to an Erlenmeyer flask in an ice-bath with a minimum volume of methanol and diluted with water (10-fold of solvent volume). The pH was brought to ~8 with ammonium hydroxide solution (25%) resulting in precipitate formation. The mixture was held on ice for 15–60 min and then filtered over filter paper; washing with distilled water. The residue was dried under vacuum to afford the desired thienopyrimidine in sufficient purity for the subsequent step. Due to the poor solubility of these compounds, full characterization was performed after the next synthetic step and purification.

Ethyl 2-((diethoxyphosphoryl)methyl)-5-methyl-4-oxo-3,4-dihydrothieno[2,3-d]pyrimidine-6-carboxylate (8)

A 100 mL RBF was charged with ethyl 2-(chloromethyl)-5-methyl-4-oxo-3,4-dihydrothieno[2,3-d]pyrimidine-6-carboxylate (900 mg, 3.13 mmol) (**6**) and triethylphosphite (10.4 g, 10.8 mL, 62.8 mmol) was added *via* syringe and the reaction was heated at 145 °C for 2 h. The reaction mixture was cooled down, diluted with 100 mL diethyl ether and stirred for 1 h on ice. The suspension was filtered, washed with copious amounts of ether and petroleum ether. The obtained residue was dried on high vacuum to furnish the desired the product as a fine, free-flowing white powder, 994 mg (82%). ^{1}H NMR (500 MHz, DMSO) δ 12.62 (s, NH), 4.28 (q, J = 7.1 Hz, 2H), 4.10 – 3.99 (m, 4H), 3.37 (d, J = 22.2 Hz, 2H), 2.79 (s, 3H), 1.28 (t, J = 7.1 Hz, 3H), 1.21 (t, J = 7.0 Hz, 6H). ^{13}C NMR (126 MHz, DMSO) δ 166.99 (d, J = 3.0 Hz), 162.98, 159.97, 154.77 (d, J = 8.6 Hz), 144.46, 122.93, 122.17, 63.42 (d, J = 6.3 Hz), 62.28, 33.99 (d, J = 131.2 Hz), 17.30 (d, J = 6.0 Hz), 15.95, 15.29. ^{31}P NMR (121 MHz, DMSO) δ 21.87. MS (ESI): calcd. 389.09; found 389.07 $[M+H]^{+}$.

General procedure for the Horner-Wadsworth-Emmons reactions

To an ice-cooled solution of phosphonate **8** (1 equivalent) and aldehyde (3 equivalents) in anhydrous THF was added sodium hydride (60% suspension in mineral oil, 3 equivalents) in small portions. The reaction was stirred at RT until complete consumption of starting material, as determined by TLC. The crude product was poured into ice-water (5 times the reaction solvent volume), filtered and washed with water. The filter-cake was washed with ice-cold ethanol, diethyl ether and pentanes. The residue was dried on high vacuum to furnish the desired product in sufficient purity for subsequent reactions.

General procedure for the hydrogenation reactions

A round bottom flask was charged with the alkene product from the HWE reaction, suspended in MeOH/THF/NH_4OH 10:2:1 and purged with nitrogen. Pearlman's catalyst was

added (20% $Pd(OH)_2/C$, 0.5 equivalents, CAS 12135-22-7), and the reaction mixture was purged with H_2 gas and equipped with an H_2-filled balloon. The reaction was stirred at 60°C until complete consumption of starting material, as determined by TLC, replenishing the H_2 balloon as needed. The reaction mixture was purged with nitrogen and filtered through a plug of Celite, rinsing with EtOAc. The filtrate was concentrated *in vacuo* and the obtained material was used without further purification.

General procedure for the formation of ester precursors (10)

To a solution of or thienopyrimidinone (1 equivalent) and (benzotriazol-1-yloxy)-tripyrrolidinophosphonium hexafluorophosphate (PyBOP, 1.3 equivalents) in anhydrous acetonitrile was added 1,8-diazabicyclo[5.4.0]undec-7-ene (1.5 equivalents, 3 equivalents in case of amine-HCl salts) *via* syringe. The mixture was stirred at RT for 5 min, after which the nucleophile (1.5 equivalents) was added and the reaction stirred at RT until complete consumption of starting material, as determined by TLC. The solvent was removed *in vacuo* and the crude residue was purified by column chromatography on silica gel using a gradient of EtOAc in 1:1 Hex/CH_2Cl_2. *Note*: Substituent **b** was introduced as a mono-Boc-protected diamine; the Boc protecting group was expediently removed by treating the compound with 4 M HCl in 1,4-dioxane followed by precipitation with cold diethyl ether and filtration.

Ethyl 5-methyl-4-(methylamino)-2-phenethylthieno[2,3-d]pyrimidine-6-carboxylate 10(d,a)

Isolated 80 mg (77% yield) as a white solid. ^{1}H NMR (500 MHz, DMSO) δ 7.27 – 7.19 (m, 4H), 7.17 – 7.12 (m, 1H), 7.09 (m, NH), 4.28 (q, J = 7.1 Hz, 2H), 3.09 – 3.04 (m, 2H), 3.02 – 2.97 (m, 5H), 2.86 (s, 3H), 1.28 (t, J = 7.1 Hz, 3H). ^{13}C NMR (126 MHz, DMSO) δ 168.26, 167.97, 163.50, 159.84, 142.72, 141.08, 129.47, 129.39, 126.92, 120.08, 115.95, 62.16, 41.31, 34.42, 29.27, 16.74, 15.34. MS (ESI): calcd. 356.14; found 356.27 $[M+H]^+$.

Ethyl 4-((2-aminoethyl)amino)-5-methyl-2-phenethylthieno[2,3-d]pyrimidine-6-carboxylate 10(d,b)

Isolated 70 mg (92% yield) as a white powder. ^{1}H NMR (500 MHz, DMSO) δ 8.00 (br. s., NH_2), 7.48 (m, NH), 7.29 – 7.24 (m, 4H), 7.19 – 7.14 (m, 1H), 4.30 (q, J = 7.1 Hz, 2H), 3.81 (q, J = 5.6 Hz, 2H), 3.12 – 3.03 (m, 6H), 2.95 (s, 3H), 1.30 (t, J = 7.1 Hz, 3H).^{13}C NMR (75 MHz, DMSO) δ 165.02, 162.48, 159.04, 141.38, 140.89, 129.04, 128.98, 126.75, 121.53, 116.43, 62.15, 38.60, 38.41, 33.27, 16.21, 14.79. MS (ESI): calcd. 385.170; found 385.20 $[M+H]^+$.

Ethyl 4-(benzylamino)-5-methyl-2-phenethylthieno[2,3-d]pyrimidine-6-carboxylate 10(d,c)

Isolated 80 mg (79% yield) as an off-white solid. ^{1}H NMR (500 MHz, DMSO) δ 7.70 (m, NH_2), 7.40 (d, J = 7.7 Hz, 2H), 7.29 (t, J = 7.6 Hz, 2H), 7.23 – 7.15 (m, 3H), 7.09 (m, 3H), 4.75 (d, J = 5.8 Hz, 2H), 4.27 (q, J = 7.1 Hz, 2H), 2.93 (m, 7H), 1.28 (t, J = 7.1 Hz, 3H). ^{13}C NMR (126 MHz, DMSO) δ 168.26, 168.09, 163.46, 159.24, 142.59, 141.04, 140.88, 129.38, 129.33, 128.52, 127.77, 126.85, 120.39, 115.86, 62.19, 45.07, 41.25, 34.27, 16.88, 15.31. MS (ESI): calcd. 432.17; found 432.33 $[M+H]^+$.

Ethyl 5-methyl-2-phenethyl-4-(phenethylamino)thieno[2,3-d]pyrimidine-6-carboxylate 10(d,d)

Isolated 106 mg (91% yield) as a pale yellow solid. ^{1}H NMR (500 MHz, DMSO) δ 7.32 – 7.16 (m, 8H & NH), 7.16 – 7.07 (m, 2H), 4.26 (q, *J* = 7.0 Hz, 2H), 3.72 (dd, *J* = 14.0, 6.3 Hz, 2H), 3.13 – 3.05 (m, 2H), 3.05 – 2.96 (m, 2H), 2.94 – 2.86 (m, 2H), 2.79 (s, 3H), 1.27 (t, *J* = 7.1 Hz, 3H). ^{13}C NMR (126 MHz, DMSO) δ 168.22, 168.19, 163.44, 159.23, 142.67, 140.85, 140.67, 129.82, 129.55, 129.40, 129.37, 127.29, 126.93, 120.27, 115.77, 62.14, 43.49, 41.29, 35.77, 34.47, 16.60, 15.30. MS (ESI): calcd. 446.19; found 446.40 $[M+H]^{+}$.

Ethyl 4-((4-methoxyphenethyl)amino)-5-methyl-2-phenethylthieno[2,3-d]pyrimidine-6-carboxylate 10(d,g)

Isolated 172 mg (83% yield) as an off-white solid. ^{1}H NMR (500 MHz, DMSO) δ 7.26 – 7.20 (m, 4H), 7.18 – 7.09 (m, 3H & NH), 6.86 (d, *J* = 8.6 Hz, 2H), 4.28 (q, *J* = 7.1 Hz, 2H), 3.71 – 3.66 (m, 5H), 3.12 – 3.07 (m, 2H), 3.03 – 2.99 (m, 2H), 2.86 – 2.80 (m, 5H), 1.28 (t, *J* = 7.1 Hz, 3H). ^{13}C NMR (75 MHz, $CDCl_3$) δ 168.07, 163.30, 158.99, 158.70, 142.08, 138.32, 130.92, 130.03, 128.70, 128.55, 126.07, 121.47, 115.33, 114.46, 61.45, 55.53, 42.47, 41.16, 34.55, 34.46, 15.70, 14.58. MS (ESI): calcd. 476.20; found 476.40 $[M+H]^{+}$.

Ethyl 4-((3-methoxyphenethyl)amino)-5-methyl-2-phenethylthieno[2,3-d]pyrimidine-6-carboxylate 10(d,h)

Isolated 182 mg (87% yield) as a pale yellow solid. ^{1}H NMR (500 MHz, DMSO) δ 7.27 – 7.19 (m, 6H), 7.17 – 7.11 (m, 1H 7 NH), 6.82 (m, 2H), 4.28 (q, *J* = 7.1 Hz, 2H), 3.73 (m, 2H), 3.69 (s, 3H), 3.10 (m, 2H), 3.01 (m, 2H), 2.91 – 2.86 (m, 2H), 2.82 (s, 3H), 1.28 (t, *J* = 7.1 Hz, 3H). ^{13}C NMR (75 MHz, $CDCl_3$) δ 168.05, 163.28, 160.23, 158.96, 142.08, 140.67, 138.35, 130.10, 128.70, 128.56, 126.08, 121.47, 121.36, 115.34, 114.92, 112.13, 61.45, 55.39, 42.27, 41.18, 35.41, 34.56, 15.66, 14.58. MS (ESI): calcd. 476.20; found 476.47 $[M+H]^{+}$.

Ethyl 4-((2-methoxyphenethyl)amino)-5-methyl-2-phenethylthieno[2,3-d]pyrimidine-6-carboxylate 10(d,i)

Isolated 198 mg (95% yield) as a beige solid. ^{1}H NMR (500 MHz, DMSO) δ 7.25 – 7.11 (m, 7H), 7.08 (m, NH), 6.95 (d, *J* = 7.6 Hz, 1H), 6.86 (td, *J* = 7.4, 1.0 Hz, 1H), 4.28 (q, *J* = 7.1 Hz, 2H), 3.74 (s, 3H), 3.73 – 3.68 (m, 2H), 3.09 (m, 2H), 3.00 (m, 2H), 2.92 (t, *J* = 7.3 Hz, 2H), 2.81 (s, 3H), 1.30 – 1.26 (m, 3H). ^{13}C NMR (75 MHz, $CDCl_3$) δ 168.04, 163.38, 159.12, 157.72, 142.17, 138.59, 130.92, 128.72, 128.54, 128.39, 127.51, 126.04, 121.11, 115.32, 110.79, 61.40, 55.61, 41.84, 41.19, 34.53, 29.65, 15.62, 14.59. MS (ESI): calcd. 476.20; found 476.27 $[M+H]^{+}$.

Ethyl 4-((4-fluorophenethyl)amino)-5-methyl-2-phenethylthieno[2,3-d]pyrimidine-6-carboxylate 10(d,j)

Isolated 183 mg (90% yield) as a pale yellow solid. ^{1}H NMR (300 MHz, $CDCl_3$) δ 7.32 – 7.23 (m, 4H), 7.21 – 7.12 (m, 3H), 7.02 (m, 2H), 5.61 (t, *J* = 5.5 Hz, NH), 4.34 (q, *J* = 7.1 Hz, 2H), 3.85 (dd, *J* = 12.5, 6.8 Hz, 2H), 3.22 – 3.14 (m, 4H), 2.94 (m, 2H), 2.71 (s, 3H), 1.38 (t, *J* = 7.1 Hz, 3H). ^{13}C NMR (75 MHz, $CDCl_3$) δ 168.02, 163.25, 161.95 (d, *J* = 245.0

Hz), 158.92, 142.03, 138.10, 134.79 (d, J = 3.3 Hz), 130.55, 130.44, 128.67, 128.57, 126.09, 121.68, 115.82 (d, J = 21.2 Hz), 115.30, 61.49, 42.44, 41.14, 34.63, 34.54, 15.71, 14.57. MS (ESI): calcd. 464.18; found 464.47 $[M+H]^+$.

Ethyl 4-((3-fluorophenethyl)amino)-5-methyl-2-phenethylthieno[2,3-d]pyrimidine-6-carboxylate 10(d,k)

Isolated 168 mg (83% yield) as a pale yellow solid. ^{1}H NMR (300 MHz, $CDCl_3$) δ 7.34 – 7.23 (m, 5H), 7.18 (m, 1H), 7.05 – 6.89 (m, 3H), 5.63 (t, J = 5.4 Hz, NH), 4.34 (q, J = 7.1 Hz, 2H), 3.87 (dd, J = 12.5, 6.8 Hz, 2H), 3.23 – 3.15 (m, 4H), 2.96 (m, 2H), 2.72 (s, 3H), 1.38 (t, J = 7.1 Hz, 3H). ^{13}C NMR (75 MHz, $CDCl_3$) δ 168.01, 163.27 (d, J = 246.3 Hz), 163.23, 158.88, 142.02, 141.77 (d, J = 7.1 Hz), 138.14, 130.49 (d, J = 8.3 Hz), 128.68, 128.57, 126.09, 124.78, 124.75, 121.68, 115.90 (d, J = 20.9 Hz), 115.31, 113.88 (d, J = 21.0 Hz), 61.48, 42.17, 41.16, 35.21, 34.56, 15.69, 14.57. MS (ESI): calcd. 464.18; found 464.47 $[M+H]^+$.

Ethyl 4-((2-fluorophenethyl)amino)-5-methyl-2-phenethylthieno[2,3-d]pyrimidine-6-carboxylate 10(d,l)

Isolated 170 mg (84% yield) as an off-white solid. ^{1}H NMR (300 MHz, $CDCl_3$) δ 7.32 – 7.02 (m, 9H), 5.69 (t, J = 5.4 Hz, NH), 4.35 (q, J = 7.1 Hz, 2H), 3.89 (dd, J = 12.4, 6.6 Hz, 2H), 3.23 – 3.12 (m, 4H), 3.04 (m, 2H), 2.76 (s, 3H), 1.39 (t, J = 7.1 Hz, 3H). ^{13}C NMR (75 MHz, $CDCl_3$) δ 168.00, 163.30, 161.51 (d, J = 244.8 Hz), 158.99, 142.10, 138.29, 131.46 (d, J = 4.9 Hz), 128.86, 128.75, 128.70, 128.55, 126.08 (d, J = 16.0 Hz), 126.06, 124.60 (d, J = 3.5 Hz), 121.55, 115.75 (d, J = 22.0 Hz), 115.31, 61.46, 41.41, 41.16, 34.52, 29.03, 15.68, 14.58. MS (ESI): calcd. 464.18; found 464.47 $[M+H]^+$.

Ethyl 5-methyl-4-((4-methylphenethyl)amino)-2-phenethylthieno[2,3-d]pyrimidine-6-carboxylate 10(d,m)

Isolated 103 mg (77% yield) as a white solid. ^{1}H NMR (300 MHz, $CDCl_3$) δ 7.34 – 7.10 (m, 9H), 5.61 (t, J = 5.3 Hz, NH), 4.35 (q, J = 7.1 Hz, 2H), 3.88 (dd, J = 12.2, 6.6 Hz, 2H), 3.24 – 3.13 (m, 4H), 2.95 (t, J = 6.7 Hz, 2H), 2.69 (s, 3H), 2.36 (s, 3H), 1.40 (t, J = 7.1 Hz, 3H). ^{13}C NMR (75 MHz, $CDCl_3$) δ 168.09, 163.33, 159.00, 142.11, 138.36, 136.59, 135.89, 129.76, 128.96, 128.71, 128.56, 126.07, 121.45, 115.34, 61.44, 42.41, 41.19, 34.93, 34.57, 21.32, 15.68, 14.59. MS (ESI): calcd. 460.21; found 460.47 $[M+H]^+$.

Ethyl 5-methyl-4-((3-methylphenethyl)amino)-2-phenethylthieno[2,3-d]pyrimidine-6-carboxylate 10(d,n)

Isolated 113 mg (84% yield) as an off-white solid. ^{1}H NMR (300 MHz, $CDCl_3$) δ 7.34 – 7.16 (m, 6H), 7.07 (m, 3H), 5.61 (t, J = 5.3 Hz, NH), 4.35 (q, J = 7.1 Hz, 2H), 3.89 (dd, J = 12.2, 6.6 Hz, 2H), 3.19 (m, 4H), 2.95 (t, J = 6.7 Hz, 2H), 2.69 (s, 3H), 2.36 (s, 3H), 1.39 (t, J = 7.1 Hz, 3H). ^{13}C NMR (75 MHz, $CDCl_3$) δ 168.09, 163.31, 159.00, 142.11, 138.97, 138.74, 138.33, 129.89, 129.03, 128.71, 128.56, 127.79, 126.09, 126.07, 121.46, 115.36, 61.45, 42.36, 41.20, 35.29, 34.58, 21.66, 15.61, 14.58. MS (ESI): calcd. 460.21; found 460.50 $[M+H]^+$.

Ethyl 5-methyl-4-((2-methylphenethyl)amino)-2-phenethylthieno[2,3-d]pyrimidine-6-carboxylate 10(d,o)

Isolated 101 mg (75% yield) as a pale yellow solid. ^{1}H NMR (300 MHz, $CDCl_3$) δ 7.33 – 7.14 (m, 9H), 5.68 (t, *J* = 5.5 Hz, NH), 4.36 (q, *J* = 7.1 Hz, 2H), 3.87 (dd, *J* = 12.8, 7.0 Hz, 2H), 3.19 (m, 4H), 3.01 (t, *J* = 7.1 Hz, 2H), 2.76 (s, 3H), 2.41 (s, 3H), 1.40 (t, *J* = 7.1 Hz, 3H). ^{13}C NMR (75 MHz, $CDCl_3$) δ 168.10, 163.32, 159.09, 142.07, 138.29, 137.10, 136.71, 130.94, 129.79, 128.70, 128.57, 127.16, 126.48, 126.09, 121.56, 115.35, 61.47, 41.30, 41.13, 34.69, 32.99, 19.71, 15.79, 14.59. MS (ESI): calcd. 460.21; found 460.47 $[M+H]^+$.

Ethyl 5-methyl-2-phenethyl-4-((2-(pyridin-4-yl)ethyl)amino)thieno[2,3-d]pyrimidine-6-carboxylate 10(d,p)

Isolated 70 mg (72% yield) as a pale yellow solid. ^{1}H NMR (500 MHz, DMSO) δ 8.45 (d, *J* = 5.9 Hz, 2H), 7.25 (d, *J* = 6.0 Hz, 2H), 7.22 (m, 4H), 7.18 (br. t, *J* = 5.8 Hz, NH), 7.13 (m, 1H), 4.28 (q, *J* = 7.1 Hz, 2H), 3.77 (dd, *J* = 13.5, 6.5 Hz, 2H), 3.10 – 3.05 (m, 2H), 3.03 – 2.98 (m, 2H), 2.92 (dd, *J* = 10.3, 4.0 Hz, 2H), 2.81 (s, 3H), 1.29 (t, *J* = 7.1 Hz, 3H). ^{13}C NMR (126 MHz, DMSO) δ 168.27, 159.30, 150.69, 149.70, 140.91, 129.45, 127.00, 125.50, 62.28, 42.30, 35.00, 34.48, 16.68, 15.37. MS (ESI): calcd. 447.185; found 447.20 $[M+H]^+$.

Ethyl 5-methyl-2-phenethyl-4-((2-(pyridin-3-yl)ethyl)amino)thieno[2,3-d]pyrimidine-6-carboxylate 10(d,q)

Isolated 54 mg (41% yield) as a pale yellow solid. ^{1}H NMR (500 MHz, DMSO) δ 8.46 (s, 1H), 8.41 (d, *J* = 4.5 Hz, 1H), 7.64 (d, *J* = 7.8 Hz, 1H), 7.31 (dd, *J* = 7.7, 4.8 Hz, 1H), 7.25 – 7.21 (m, 4H), 7.19 – 7.12 (m, NH, 1H), 4.28 (q, *J* = 7.1 Hz, 2H), 3.76 (dd, *J* = 13.1, 6.7 Hz, 2H), 3.10 – 3.05 (m, 2H), 3.00 (dd, *J* = 8.4, 6.2 Hz, 2H), 2.93 (t, *J* = 7.1 Hz, 2H), 2.81 (s, 3H), 1.29 (t, *J* = 7.1 Hz, 3H). ^{13}C NMR (126 MHz, DMSO) δ 168.19, 163.47, 159.26, 151.00, 148.56, 142.66, 140.86, 137.49, 136.20, 129.41, 126.95, 124.63, 120.37, 115.78, 62.21, 42.92, 41.25, 34.48, 32.87, 16.65, 15.32. MS (ESI): calcd. 447.185; found 447.27 $[M+H]^+$.

Ethyl 5-methyl-2-phenethyl-4-((2-(pyridin-2-yl)ethyl)amino)thieno[2,3-d]pyrimidine-6-carboxylate 10(d,r)

Isolated 118 mg (90% yield) as a pale yellow solid. ^{1}H NMR (300 MHz, $CDCl_3$) δ 8.52 (dd, *J* = 5.8, 1.7 Hz, 1H), 7.62 (td, *J* = 7.7, 1.8 Hz, 1H), 7.49 (s, NH), 7.31 – 7.23 (m, 4H), 7.21 – 7.13 (m, 3H), 4.34 (q, *J* = 7.1 Hz, 2H), 4.02 (dd, *J* = 11.5, 5.2 Hz, 2H), 3.19 – 3.06 (m, 6H), 2.97 (s, 3H), 1.38 (t, *J* = 7.1 Hz, 3H). ^{13}C NMR (75 MHz, $CDCl_3$) δ 168.08, 168.01, 163.46, 160.33, 158.80, 149.13, 142.21, 139.20, 137.12, 128.71, 128.51, 126.00, 123.76, 122.02, 120.96, 115.53, 61.35, 41.19, 40.27, 36.09, 34.56, 15.79, 14.60. MS (ESI): calcd. 447.19; found 447.40 $[M+H]^+$.

Ethyl 4-((2,3-dihydro-1H-inden-2-yl)amino)-5-methyl-2-phenethylthieno[2,3-d]pyrimidine-6-carboxylate 10(d,x)

Isolated 105 mg (79% yield) as a pale yellow solid. ^{1}H NMR (300 MHz, $CDCl_3$) δ 7.33 – 7.17 (m, 9H), 5.82 (d, *J* = 6.7 Hz, NH), 5.13 (m, 1H), 4.36 (q, *J* = 7.1 Hz, 2H), 3.52 (d, *J* = 7.3 Hz, 2H), 3.46 (d, *J* = 7.2 Hz, 2H), 2.95 (d, *J* = 5.4 Hz, 2H), 2.89 (d, *J* = 5.5 Hz, 2H), 2.84

(s, 3H), 1.40 (t, J = 7.1 Hz, 3H). ^{13}C NMR (75 MHz, $CDCl_3$) δ 168.03, 163.28, 158.79, 142.05, 141.03, 138.10, O128.71, 128.57, 127.14, 126.08, 125.10, 121.73, 115.31, 61.49, 52.48, 41.12, 40.45, 34.57, 15.88, 14.58. MS (ESI): calcd. 458.19; found 458.47 $[M+H]^+$.

Ethyl 4-((3,5-dimethoxyphenethyl)amino)-5-methyl-2-phenethylthieno[2,3-d]pyrimidine-6-carboxylate 10(d,y)

Isolated 77 mg (52% yield) as a pale yellow solid. ^{1}H NMR (500 MHz, DMSO) δ 7.23 (m, 4H), 7.16 – 7.09 (m, 1H, NH), 6.41 (s, 2H), 6.33 (s, 1H), 4.28 (q, J = 7.1 Hz, 2H), 3.73 (dd, J = 13.7, 6.3 Hz, 2H), 3.67 (s, 6H), 3.10 (m, 2H), 3.04 – 2.98 (m, 2H), 2.88 – 2.79 (m, 5H), 1.29 (t, J = 7.1 Hz, 3H). ^{13}C NMR (126 MHz, DMSO) δ 168.21, 168.18, 163.44, 161.61, 159.23, 142.96, 142.67, 140.85, 129.39, 129.37, 126.94, 120.26, 115.78, 107.80, 99.12, 62.15, 56.10, 43.39, 41.34, 36.05, 34.48, 16.60, 15.29. MS (ESI): calcd. 506.21; found 506.53 $[M+H]^+$

Ethyl 4-((2-(benzo[d][1,3]dioxol-5-yl)ethyl)amino)-5-methyl-2-phenethylthieno[2,3-d]pyrimidine-6-carboxylate 10(d,z)

Isolated 94 mg (66% yield) as a pale yellow solid. ^{1}H NMR (500 MHz, DMSO) δ 7.27 – 7.20 (m, 4H), 7.10 (s, 1H, NH), 6.85 – 6.79 (m, 2H), 6.68 (d, J = 7.9 Hz, 1H), 5.95 (s, 2H), 4.28 (q, J = 7.1 Hz, 2H), 3.69 (dd, J = 14.1, 6.3 Hz, 2H), 3.12 – 3.05 (m, 2H), 3.05 – 2.95 (m, 2H), 2.85 – 2.78 (m, 5H), 1.29 (t, J = 7.1 Hz, 3H). ^{13}C NMR (126 MHz, DMSO) δ 168.19, 163.45, 159.23, 148.42, 146.70, 142.67, 140.87, 134.41, 129.40, 129.38, 126.94, 122.67, 120.25, 115.76, 110.12, 109.30, 101.84, 62.15, 43.63, 41.32, 35.45, 34.49, 16.62, 15.31. MS (ESI): calcd. 490.18; found 490.47 $[M+H]^+$.

Ethyl 5-methyl-4-(methylamino)-2-(3-phenylpropyl)thieno[2,3-d]pyrimidine-6-carboxylate 10(e,a)

Isolated 52 mg (33% yield) as a yellow oil. ^{1}H NMR (300 MHz, $CDCl_3$) δ 7.26 – 7.14 (m, 5H), 5.67 (m, NH), 4.33 (q, J = 7.1 Hz, 2H), 3.12 (d, J = 4.8 Hz, 3H), 2.88 (s, 3H), 2.84 (m, 2H), 2.75 – 2.67 (m, 2H), 2.22 – 2.11 (m, 2H), 1.37 (t, J = 7.1 Hz, 3H). ^{13}C NMR (75 MHz, $CDCl_3$) δ 168.72, 167.83, 163.32, 159.61, 142.63, 138.32, 128.75, 128.45, 125.88, 121.25, 115.33, 61.42, 39.21, 35.91, 30.26, 28.33, 15.93, 14.56. MS (ESI): calcd. 370.159; found 370.33 $[M+H]^+$

Ethyl 5-methyl-4-(methylamino)-2-(4-phenylbutyl)thieno[2,3-d]pyrimidine-6-carboxylate 10(f,a)

Isolated 88 mg (43 % yield) as a pale yellow syrup. ^{1}H NMR (300 MHz, $CDCl_3$) δ 7.29 – 7.13 (m, 5H), 5.64 (br. m, NH), 4.34 (q, J = 7.1 Hz, 2H), 3.11 (d, J = 4.8 Hz, 3H), 2.89 (s, 3H), 2.88 – 2.81 (m, 2H), 2.70 – 2.63 (m, 2H), 1.95 – 1.83 (m, 2H), 1.78 – 1.67 (m, 2H), 1.38 (t, J = 7.1 Hz, 3H). ^{13}C NMR (75 MHz, $CDCl_3$) δ 168.96, 167.88, 163.35, 159.64, 142.89, 138.27, 128.65, 128.43, 125.80, 121.27, 115.32, 61.42, 39.51, 36.06, 31.51, 28.30, 15.95, 14.57. MS (ESI): calcd. 384.175; found 384.27 $[M+H]^+$.

Ethyl 2-(3-methoxyphenethyl)-5-methyl-4-(methylamino)thieno[2,3-d]pyrimidine-6-carboxylate 10(h,a)

Isolated 163 mg (83% yield) as a pale yellow solid. ^{1}H NMR (300 MHz, $CDCl_3$) δ 7.16 (t, *J* = 7.8 Hz, 1H), 6.84 (m, 2H), 6.70 (dd, *J* = 8.1, 2.5 Hz, 1H), 5.66 (br. m, NH), 4.33 (q, *J* = 7.1 Hz, 2H), 3.75 (s, 3H), 3.15 – 3.08 (m, 7H), 2.86 (s, 3H), 1.37 (t, *J* = 7.1 Hz, 3H). ^{13}C NMR (75 MHz, $CDCl_3$) δ 167.96, 163.29, 159.77, 159.61, 143.75, 138.29, 129.46, 121.37, 121.09, 115.41, 114.25, 111.53, 61.44, 55.32, 41.06, 34.48, 28.32, 15.90, 14.56. MS (ESI): calcd. 386.154; found 386.27 $[M+H]^+$.

Ethyl 2-(3-fluorophenethyl)-5-methyl-4-(methylamino)thieno[2,3-d]pyrimidine-6-carboxylate 10(k,a)

Isolated 141 mg (54% yield) as a pale yellow oil. ^{1}H NMR (300 MHz, $CDCl_3$) δ 7.21 – 7.13 (m, 1H), 7.05 – 6.92 (m, 2H), 6.84 (td, *J* = 8.5, 2.6 Hz, 1H), 5.66 (br. m, NH), 4.33 (q, *J* = 7.1 Hz, 2H), 3.17 – 3.06 (m, 7H), 2.88 (s, 3H), 1.37 (t, *J* = 7.1 Hz, 3H). ^{13}C NMR (75 MHz, $CDCl_3$) δ 167.80, 167.58, 164.66, 163.28, 161.41, 159.61, 144.70 (d, *J* = 7.2 Hz), 138.21, 129.85 (d, *J* = 8.4 Hz), 124.34 (d, *J* = 2.6 Hz), 121.51, 115.42 (d, *J* = 3.6 Hz), 112.84 (d, *J* = 21.0 Hz), 61.46, 40.67, 34.02, 28.32, 15.92, 14.54. MS (ESI): calcd. 374.134; found 374.20 $[M+H]^+$.

Ethyl 5-methyl-4-(methylamino)-2-(2-(pyridin-2-yl)ethyl)thieno[2,3-d]pyrimidine-6-carboxylate 10(q,a)

Isolated 585 mg (57% yield) as a white solid. ^{1}H NMR (300 MHz, $CDCl_3$) δ 8.54 (ddd, *J* = 5.0, 1.7, 0.8 Hz, 1H), 7.65 (td, *J* = 7.7, 1.8 Hz, 1H), 7.29 (d, *J* = 7.9 Hz, 1H), 7.17 (ddd, *J* = 7.5, 5.0, 1.1 Hz, 1H), 5.68 (br. m, NH), 4.34 (q, *J* = 7.1 Hz, 2H), 3.45 – 3.35 (m, 2H), 3.29 (m, 2H), 3.08 (d, *J* = 4.7 Hz, 3H), 2.91 (s, 3H), 1.38 (t, *J* = 7.1 Hz, 3H). ^{13}C NMR (75 MHz, $CDCl_3$) δ 167.41, 163.29, 161.18, 159.61, 148.18, 138.21, 137.73, 123.64, 121.71, 121.59, 115.48, 61.47, 38.68, 35.79, 28.39, 15.96, 14.55. MS (ESI): calcd. 357.139; found 357.20 $[M+H]^+$.

Ethyl 2-(4-acetamidophenethyl)-5-methyl-4-(methylamino)thieno[2,3-d]pyrimidine-6-carboxylate 10(s,a)

Isolated 38 mg (68% yield) as a beige solid. ^{1}H NMR (500 MHz, DMSO) δ 9.83 (s, NHAc), 7.41 (d, *J* = 8.4 Hz, 2H), 7.13 (d, *J* = 8.2 Hz, 2H), 7.09 (m, NH), 4.27 (q, *J* = 7.1 Hz, 2H), 3.02 – 2.94 (m, 7H), 2.86 (s, 3H), 1.98 (s, 3H), 1.28 (t, *J* = 7.1 Hz, 3H). ^{13}C NMR (126 MHz, $CDCl_3$ + CD_3OD) δ 174.50, 172.26, 171.43, 167.85, 164.01, 143.40, 142.04, 140.74, 133.30, 125.53, 124.67, 119.90, 65.95, 45.18, 38.26, 32.49, 28.11, 19.95, 18.70. MS (ESI): calcd. 413.16; found 413.33 $[M+H]^+$.

Ethyl 2-(4-acetamidophenethyl)-4-((2-aminoethyl)amino)-5-methylthieno[2,3-d]pyrimidine-6-carboxylate 10(s,b)

Isolated 51 mg (83 % yield) as a white solid. ^{1}H NMR (300 MHz, DMSO) δ 9.81 (s, NHAc), 7.43 (d, *J* = 8.4 Hz, 2H), 7.14 (d, *J* = 8.4 Hz, 2H), 7.07 – 6.96 (m, NH), 4.26 (q, *J* = 7.0 Hz, 2H), 3.57 (dd, *J* = 11.0, 5.5 Hz, 2H), 3.23 (dd, *J* = 11.6, 6.1 Hz, 2H), 3.03 – 2.90 (m, 4H), 2.86 (s, 3H), 1.99 (s, 3H), 1.27 (t, *J* = 7.1 Hz, 3H). ^{13}C NMR (75 MHz, DMSO) δ

167.69, 162.98, 159.06, 156.71, 140.62, 137.83, 136.80, 129.09, 119.63, 115.35, 78.38, 61.67, 33.38, 24.59, 21.41, 16.11, 14.81. MS (ESI): calcd. 442.191; found 442.27 $[M+H]^+$.

Ethyl 2-(4-acetamidophenethyl)-5-methyl-4-((2-(pyridin-4-yl)ethyl)amino)thieno[2,3-d]pyrimidine-6-carboxylate 10(s,p)

Isolated 86 mg (68% yield) as a pale yellow solid. ^{1}H NMR (500 MHz, DMSO) δ 9.83 (s, NHAc), 8.46 (d, *J* = 4.7 Hz, 2H), 7.45 (d, *J* = 8.2 Hz, 2H), 7.24 (m, 2H, NH), 7.12 (d, *J* = 8.2 Hz, 2H), 4.26 (q, *J* = 7.0 Hz, 2H), 3.76 (dd, *J* = 12.7, 6.4 Hz, 2H), 3.07 – 2.90 (m, 6H), 2.79 (s, 3H), 2.00 (s, 3H), 1.28 (t, *J* = 7.0 Hz, 3H). ^{13}C NMR (126 MHz, DMSO) δ 169.24, 168.18, 163.44, 159.18, 150.63, 149.67, 140.79, 138.35, 137.19, 129.51, 129.43, 129.38, 125.41, 120.15, 115.75, 62.17, 46.92, 41.32, 34.98, 33.91, 25.05, 16.61, 15.28. MS (ESI): calcd. 504.207; found 504.13 $[M+H]^+$.

Ethyl 2-(4-acetamidophenethyl)-5-methyl-4-((2-(pyridin-3-yl)ethyl)amino)thieno[2,3-d]pyrimidine-6-carboxylate 10(s,q)

Isolated 79 mg (63% yield) as a pale yellow solid. ^{1}H NMR (500 MHz, DMSO) δ 9.83 (s, NHAc), 8.41 (d, *J* = 4.7 Hz, 1H), 7.63 (d, *J* = 7.7 Hz, 1H), 7.46 (m, *J* = 15.7, 8.4 Hz, 3H), 7.30 (dd, *J* = 7.7, 4.8 Hz, 1H), 7.18 – 7.10 (m, 2H, NH), 4.27 (q, *J* = 7.0 Hz, 2H), 3.76 (dd, *J* = 12.9, 6.6 Hz, 2H), 3.06 – 2.91 (m, 6H), 2.80 (s, 3H), 2.00 (s, 3H), 1.29 (t, *J* = 7.1 Hz, 3H). ^{13}C NMR (126 MHz, DMSO) δ 168.20, 163.45, 159.23, 151.01, 148.58, 140.83, 137.41, 137.19, 136.19, 129.62, 129.52, 124.60, 120.22, 120.13, 115.75, 62.18, 47.02, 33.93, 32.88, 27.10, 25.06, 16.63, 15.30. MS (ESI): calcd. 504.207; found 504.27 $[M+H]^+$.

Ethyl 2-(4-acetamidophenethyl)-5-methyl-4-((2-(pyridin-2-yl)ethyl)amino)thieno[2,3-d]pyrimidine-6-carboxylate 10(s,r)

Isolated 55 mg (44% yield) as a pale yellow solid. ^{1}H NMR (500 MHz, DMSO) δ 9.83 (s, NHAc), 8.52 (d, *J* = 4.1 Hz, 1H), 7.71 (t, *J* = 7.6 Hz, 1H), 7.43 (m, 2H, NH), 7.28 (d, *J* = 7.4 Hz, 1H), 7.24 (dd, *J* = 7.4, 4.9 Hz, 1H), 7.14 (d, *J* = 8.3 Hz, 2H), 4.27 (q, *J* = 7.1 Hz, 2H), 3.88 (dd, *J* = 12.3, 6.4 Hz, 2H), 3.09 (m, 2H), 3.05 – 2.99 (m, 2H), 2.96 (dd, *J* = 8.2, 6.3 Hz, 2H), 2.84 (s, 3H), 2.00 (s, 3H), 1.29 (t, *J* = 7.1 Hz, 3H). ^{13}C NMR (126 MHz, DMSO) δ 169.20, 168.29, 168.13, 163.46, 160.72, 159.20, 150.13, 140.80, 138.33, 137.87, 137.24, 129.56, 124.47, 122.79, 120.33, 120.14, 115.79, 62.17, 41.60, 41.33, 37.36, 33.85, 25.09, 16.52, 15.31. MS (ESI): calcd. 504.207; found 504.20 $[M+H]^+$.

Ethyl 2-(3-acetamidophenethyl)-5-methyl-4-(methylamino)thieno[2,3-d]pyrimidine-6-carboxylate 10(t,a)

Isolated 45 mg (81% yield) as a white powder. ^{1}H NMR (500 MHz, DMSO) δ 9.84 (s, NHAc), 7.47 (s, 1H), 7.36 (d, *J* = 7.7 Hz, 1H), 7.14 (t, *J* = 7.8 Hz, 1H), 7.11 (m, *J* = 4.5 Hz, NH), 6.90 (d, *J* = 7.6 Hz, 1H), 4.28 (q, *J* = 7.1 Hz, 2H), 3.04 – 2.94 (m, 7H), 2.87 (s, 3H), 2.00 (s, 3H), 1.28 (t, *J* = 7.1 Hz, 3H). ^{13}C NMR (126 MHz, $CDCl_3$ + CD_3OD) δ 174.50, 172.26, 171.43, 167.85, 164.01, 143.40, 142.04, 140.74, 133.30, 125.53, 124.67, 119.90, 65.95, 45.18, 38.26, 32.49, 28.11, 19.95, 18.70. MS (ESI): calcd. 413.16; found 413.30 $[M+H]^+$.

Ethyl 2-(2-acetamidophenethyl)-5-methyl-4-(methylamino)thieno[2,3-d]pyrimidine-6-carboxylate 10(u,a)

Isolated 35 mg (63% yield) as a white powder. ^{1}H NMR (500 MHz, DMSO) δ 9.43 (s, NHAc), 7.29 (d, *J* = 7.8 Hz, 1H), 7.24 (d, *J* = 7.6 Hz, 1H), 7.13 (t, *J* = 7.5 Hz, 1H), 7.08 (m, NH, 1H), 4.27 (q, *J* = 7.1 Hz, 2H), 3.03 (m, 2H), 2.97 (d, *J* = 4.5 Hz, 3H), 2.93 (m, 2H), 2.86 (s, 3H), 2.03 (s, 3H), 1.27 (t, *J* = 7.1 Hz, 3H). ^{13}C NMR (126 MHz, $CDCl_3$ + CD_3OD) δ 175.11, 172.05, 171.24, 167.71, 164.02, 143.67, 139.66, 139.37, 134.36, 131.18, 130.57, 130.32, 125.54, 120.05, 66.02, 44.45, 33.67, 32.49, 28.01, 19.89, 18.71. MS (ESI): calcd. 413.16; found 413.10 $[M+H]^+$.

Ethyl 2-(3-chlorophenethyl)-5-methyl-4-(methylamino)thieno[2,3-d]pyrimidine-6-carboxylate 10(v,a)

Isolated 122 mg (47% yield) as a pale yellow oil. ^{1}H NMR (300 MHz, $CDCl_3$) δ 7.26 (m, 1H), 7.15 – 7.08 (m, 3H), 5.65 (br. m, NH), 4.32 (q, *J* = 7.1 Hz, 2H), 3.13 – 3.08 (m, 7H), 2.87 (s, 3H), 1.36 (t, *J* = 7.1 Hz, 3H). ^{13}C NMR (75 MHz, $CDCl_3$) δ 167.77, 167.51, 163.26, 159.59, 144.15, 138.23, 134.13, 129.73, 128.89, 126.89, 126.17, 121.49, 115.43, 61.46, 40.65, 33.94, 28.33, 15.91, 14.55. MS (ESI): calcd. 390.104; found 390.20 $[M+H]^+$.

Ethyl 5-methyl-4-(methylamino)-2-(3-(trifluoromethyl)phenethyl)thieno[2,3-d]pyrimidine-6-carboxylate 10(w,a)

Isolated 128 mg (50% yield) as a pale yellow semi-solid. ^{1}H NMR (300 MHz, $CDCl_3$) δ 7.52 (s, 1H), 7.37 (m, 3H), 5.66 (br. m, NH), 4.32 (q, *J* = 7.1 Hz, 2H), 3.25 – 3.11 (m, 4H), 3.09 (d, *J* = 4.8 Hz, 3H), 2.87 (s, 3H), 1.36 (t, *J* = 7.1 Hz, 3H). ^{13}C NMR (75 MHz, $CDCl_3$) δ 167.77, 167.36, 163.25, 159.60, 142.95, 138.20, 132.09, 130.62 (d, *J* = 31.9 Hz), 128.88, 125.52 (d, *J* = 3.8 Hz), 122.87 (d, *J* = 3.8 Hz), 121.55, 115.43, 61.46, 40.61, 34.04, 28.26, 15.88, 14.51. MS (ESI): calcd. 424.131; found 424.27 $[M+H]^+$.

Ethyl 2-(2-(benzo[d][1,3]dioxol-5-yl)ethyl)-5-methyl-4-(methylamino)thieno[2,3-d]pyrimidine-6-carboxylate 10(z,a)

Isolated 62 mg (41% yield) as a pale yellow solid. ^{1}H NMR (500 MHz, DMSO) δ 7.08 (m, NH), 6.81 (s, 1H), 6.76 (dd, *J* = 7.9, 2.0 Hz, 1H), 6.67 (d, *J* = 7.9 Hz, 1H), 5.92 (s, 2H), 4.27 (q, *J* = 7.1 Hz, 2H), 3.33 (s, 3H), 3.02 – 2.93 (m, 7H), 2.86 (s, 3H), 1.28 (t, *J* = 7.1 Hz, 3H). ^{13}C NMR (126 MHz, DMSO) δ 168.23, 167.95, 163.50, 159.82, 148.24, 146.36, 141.08, 136.55, 122.20, 120.06, 115.93, 109.95, 109.16, 101.71, 62.16, 41.56, 34.09, 29.27, 16.73, 15.33. MS (ESI): calcd. 400.13; found 400.40 $[M+H]^+$.

Dimethyl thiophene-2,5-dicarboxylate (13)

An ice-cooled pressure vessel was charged with thiophene-2,5-carboxylic acid (2.5 g, 14.5 mmol) and 50 mL anhydrous MeOH; thionyl chloride (4.2 mL, 58 mmol) was added dropwise via syringe and once gas evolution had ceased the vessel was tightly sealed with a Teflon screw cap. The reaction was stirred 1h at RT and 3h at 60°C. The reaction mixture was cooled to RT and stirred open to air for 1h. The crude reaction mixture was diluted with 100 mL DCM, stirred for 1h and decanted. The residue was collected by filtration and washed with DCM to obtain the desired product as a whit powder, 2.9 g (99% yield). ^{1}H

NMR (300 MHz, DMSO) δ 7.81 (s, 2H), 3.85 (s, 6H). ^{13}C NMR (126 MHz, DMSO) δ 162.40, 139.25, 134.94, 53.99.

Dimethyl 3-aminothiophene-2,5-dicarboxylate (14)

An ice-cooled round-bottom flask was charged with **12** (1.0 g, 5.0 mmol), followed by 5 mL sulfuric acid. Nitric acid (0.50 mL, 6.2 mmol) was added slowly dropwise via syringe and the reaction was stirred at RT for 1 h. The crude reaction mixture was carefully poured on ice-water and stirred for 1h. The suspension was filtered, washed with water and dried on high vacuum to furnish dimethyl 3-nitrothiophene-2,5-dicarboxylate as a white solid, 1.1 g (93% yield). ^{1}H NMR (500 MHz, DMSO) δ 8.22 (s, 1H), 3.88 (s, 6H). ^{13}C NMR (126 MHz, DMSO) δ 161.14, 159.81, 148.22, 136.58, 133.46, 129.26, 55.05, 54.53. A round-bottom flask was charged with dimethyl 3-nitrothiophene-2,5-dicarboxylate (1.0 g, 4.1 mmol), suspended in MeOH/THF 2:1 and purged with nitrogen. Pearlman's catalyst was added (286 mg, 2.0 mmol, 20% $Pd(OH)_2$/C, CAS 12135-22-7), and the reaction mixture was purged with H_2 gas and equipped with an H_2-filled balloon. The reaction was stirred at RT until complete consumption of starting material, as determined by TLC. The reaction mixture was purged with nitrogen and filtered through a plug of Celite, rinsing with EtOAc. The filtrate was concentrated *in vacuo* and the obtained material was used as such without further purification. Isolated 900 mg (100% yield) as a yellow powder. ^{1}H NMR (500 MHz, DMSO) δ 7.22 (s, 1H), 6.62 (s, NH_2), 3.80 (s, 3H), 3.74 (s, 3H). ^{13}C NMR (126 MHz, DMSO) δ 164.82, 162.69, 155.01, 136.68, 126.34, 103.33, 53.84, 52.61.

Thienopyrimidinone formation, amine coupling and ester saponification performed as described in the general procedures.

Methyl 4-(methylamino)-2-phenethylthieno[3,2-d]pyrimidine-6-carboxylate 16(d,a)

Isolated 106 mg (51% yield) as a white solid. ^{1}H NMR (500 MHz, DMSO) δ 7.98 (m, NH), 7.84 (s, 1H), 7.22 (m, 4H), 7.12 (m, 1H), 3.87 (s, 3H), 3.13 – 3.04 (m, 4H), 2.98 (d, J = 4.5 Hz, 3H). ^{13}C NMR (126 MHz, DMSO) δ 167.61, 163.19, 159.25, 158.42, 142.92, 137.95, 130.96, 129.43, 129.35, 126.84, 117.58, 54.06, 34.81, 26.99, 26.93. MS (ESI): calcd. 328.11; found 328.27 $[M+H]^+$.

Methyl 2-(3-methoxyphenethyl)-4-(methylamino)thieno[3,2-d]pyrimidine-6-carboxylate 16(h,a)

Isolated 100 mg (64% yield) as a pale yellow oil. MS (ESI): calcd. 358.123; found 358.27 $[M+H]^+$

General procedure for the saponification of esters

To solution of ester (1 equivalent) in 2:1 THF/MeOH was added 1 M NaOH (3 equivalents) and water to bring the final solvent ratio to 2:1:1 THF/MeOH/H_2O. In cases where the starting material was not fully dissolved, the solution was heated to 50 °C as necessary. The reaction was stirred at RT until complete consumption of starting material as determined by TLC. The reaction mixture was acidified to pH~3 with 1 M HCl and concentrated *in vacuo*. The resultant slurry was diluted with 5 mL water, filtered and washed successively with

deionized water, and purification grade pentane. The obtained residue was dried on high vacuum to furnish the desired free carboxylic acids.

5-Methyl-4-(methylamino)-2-phenethylthieno[2,3-d]pyrimidine-6-carboxylic acid (17)

Isolated 32 mg (87% yield) as a white powder. ^{1}H NMR (500 MHz, DMSO) δ 7.27 – 7.23 (m, 4H), 7.16 (m, 1H), 7.07 (br. d, *J* = 4.4 Hz, NH), 3.10 – 3.06 (m, 2H), 3.02 – 2.98 (m, 5H), 2.87 (s, 3H). ^{13}C NMR (126 MHz, DMSO) δ 166.82, 166.58, 164.06, 158.71, 141.62, 138.94, 128.33, 128.26, 125.79, 120.64, 115.00, 40.18, 33.32, 28.11, 15.44. HRMS (ESI): calcd. 328.11197 for $C_{17}H_{18}N_3O_2S$; found 328.1112 $[M+H]^+$.

4-((2-Aminoethyl)amino)-5-methyl-2-phenethylthieno[2,3-d]pyrimidine-6-carboxylic acid (18)

Isolated 15 mg (35% yield) as a white powder. ^{1}H NMR (500 MHz, DMSO) δ 7.28 – 7.14 (m, 4H), 7.04 (br. s, NH), 3.51 (m, 2H), 3.28 (m, 2H), 3.12 – 3.03 (m, 2H), 3.06 – 2.93 (m, 5H), 2.58 (s, 3H). ^{13}C NMR (126 MHz, DMSO) δ 166.91, 166.32, 163.82, 158.03, 142.57, 139.42, 128.65, 128.97, 126.02, 120.41, 114.63, 47.69, 41.31, 33.89, 25.16, 16.46. HRMS (ESI): calcd. 357.13852 for $C_{18}H_{21}N_4O_2S$; found 357.1389 $[M+H]^+$.

4-(Benzylamino)-5-methyl-2-phenethylthieno[2,3-d]pyrimidine-6-carboxylic acid (19)

Isolated 40 mg (86% yield) as a white crystalline material. ^{1}H NMR (500 MHz, DMSO) δ 7.96 (br. s, NH), 7.41 (d, *J* = 7.1 Hz, 2H), 7.32 (t, *J* = 7.6 Hz, 2H), 7.25 – 7.21 (m, 1H), 7.19 (d, *J* = 7.5 Hz, 2H), 7.15 – 7.08 (m, 3H), 4.79 (d, *J* = 5.8 Hz, 2H), 2.96 (m, 4H), 2.95 (s, 3H). ^{13}C NMR (126 MHz, DMSO) δ 164.72, 163.63, 157.97, 140.85, 139.07, 138.84, 128.29, 128.29, 128.25, 127.47, 126.84, 125.94, 122.31, 115.31, 44.39, 38.54, 32.66, 15.43. HRMS (ESI): calcd. 404.14327 for $C_{23}H_{22}N_3O_2S$; found 404.1432 $[M+H]^+$.

5-Methyl-2-phenethyl-4-(phenethylamino)thieno[2,3-d]pyrimidine-6-carboxylic acid (20)

Isolated 28 mg (60% yield) as a white crystalline material. ^{1}H NMR (500 MHz, DMSO) δ 7.34 – 7.19 (m, 9H), 7.17 – 7.13 (m, 1H), 7.11 (br. t, *J* = 5.7 Hz, NH), 3.74 (dd, *J* = 14.6, 6.0 Hz, 2H), 3.11 (dd, *J* = 8.5, 6.3 Hz, 2H), 3.03 (dd, *J* = 8.5, 6.2 Hz, 2H), 2.95 – 2.89 (m, 2H), 2.81 (s, 3H). ^{13}C NMR (126 MHz, DMSO) δ 166.79, 164.03, 158.14, 141.56, 139.58, 138.76, 128.73, 128.45, 128.30, 128.28, 126.19, 125.83, 120.89, 114.87, 42.33, 40.13, 34.66, 33.37, 15.33. HRMS (ESI): calcd. 418.15892 for $C_{24}H_{24}N_3O_2S$; found 418.1557 $[M+H]^+$.

4-((4-Methoxyphenethyl)amino)-5-methyl-2-phenethylthieno[2,3-d]pyrimidine-6-carboxylic acid (21)

Isolated 36 mg (55% yield) as an off white powder. ^{1}H NMR (500 MHz, DMSO) δ 7.52 (m, NH), 7.27 – 7.22 (m, 4H), 7.15 (m, *J* = 7.5 Hz, 3H), 6.86 (d, *J* = 8.7 Hz, 2H), 3.72 (dd, *J* = 14.3, 6.4 Hz, 2H), 3.70 (s, 3H), 3.13 – 3.09 (m, 2H), 3.06 (m, 2H), 2.87 – 2.82 (m, 2H), 2.82 (s, 3H). ^{13}C NMR (126 MHz, DMSO) δ 164.45, 158.96, 158.84, 141.58, 139.77, 131.93, 130.86, 129.57, 129.40, 127.30, 116.56, 115.02, 56.16, 44.42, 34.63, 33.54, 16.15. HRMS (ESI): calcd. 448.16949 for $C_{25}H_{26}N_3O_3S$; found 448.1695 $[M+H]^+$.

4-((3-Methoxyphenethyl)amino)-5-methyl-2-phenethylthieno[2,3-d]pyrimidine-6-carboxylic acid (22)

Isolated 45 mg (68% yield) as an off white powder. ^{1}H NMR (500 MHz, DMSO) δ 7.31 (m, NH), 7.25 – 7.19 (m, 5H), 7.16 – 7.12 (m, 1H), 6.81 (m, 2H), 6.77 (m, 1H), 3.75 (dd, *J* = 14.0, 6.4 Hz, 2H), 3.69 (s, 3H), 3.13 – 3.08 (m, 2H), 3.06 – 3.01 (m, 2H), 2.88 (t, *J* = 7.4 Hz, 2H), 2.81 (s, 3H). ^{13}C NMR (126 MHz, DMSO) δ 164.79, 160.49, 159.06, 142.11, 141.96, 139.82, 130.61, 129.49, 129.39, 127.13, 122.13, 116.29, 115.49, 112.80, 56.01, 43.78, 35.68, 34.00, 16.28. HRMS (ESI): calcd. 448.16949 for $C_{25}H_{26}N_3O_3S$; found 448.1684 $[M+H]^+$.

4-((2-Methoxyphenethyl)amino)-5-methyl-2-phenethylthieno[2,3-d]pyrimidine-6-carboxylic acid (23)

Isolated 28 mg (60% yield) as an off white powder. ^{1}H NMR (500 MHz, DMSO) δ 7.26 – 7.13 (m, 7H, NH), 6.95 (d, *J* = 7.7 Hz, 1H), 6.86 (t, *J* = 7.3 Hz, 1H), 3.73 (m, 5H), 3.10 (m, 2H), 3.01 (m, 2H), 2.92 (t, *J* = 7.1 Hz, 2H), 2.81 (s, 3H). ^{13}C NMR (126 MHz, DMSO) δ 164.67, 159.08, 158.45, 141.93, 139.86, 131.43, 129.53, 129.39, 128.95, 128.07, 127.19, 121.48, 116.36, 111.85, 56.38, 42.62, 33.72, 30.29, 16.20. HRMS (ESI): calcd. 448.16949 for $C_{25}H_{26}N_3O_3S$; found 448.1681 $[M+H]^+$.

4-((4-Fluorophenethyl)amino)-5-methyl-2-phenethylthieno[2,3-d]pyrimidine-6-carboxylic acid (24)

Isolated 23 mg (35% yield) as an off white powder. ^{1}H NMR (500 MHz, DMSO) δ 7.28 – 7.20 (m, 5H, NH), 7.12 (m, 4H), 3.71 (dd, *J* = 13.8, 6.2 Hz, 2H), 3.11 – 3.06 (m, 2H), 3.03 – 2.98 (m, 2H), 2.89 (t, *J* = 7.4 Hz, 2H), 2.80 (s, 3H). ^{13}C NMR (126 MHz, DMSO) δ 165.01, 162.00 (d, *J* = 241.5 Hz), 159.18, 142.45, 139.87, 136.73 (d, *J* = 3.0 Hz), 131.63 (d, *J* = 7.9 Hz), 129.44, 129.40, 127.01, 116.24 (d, *J* = 21.0 Hz), 116.08, 43.52, 34.82, 34.30, 16.41. HRMS (ESI): calcd. 436.14950 for $C_{24}H_{23}FN_3O_2S$; found 436.1473 $[M+H]^+$.

4-((3-Fluorophenethyl)amino)-5-methyl-2-phenethylthieno[2,3-d]pyrimidine-6-carboxylic acid (25)

Isolated 30 mg (46% yield) as an off white powder. ^{1}H NMR (500 MHz, DMSO) δ 7.41 (m, NH), 7.32 (dd, *J* = 14.4, 7.8 Hz, 1H), 7.26 – 7.21 (m, 4H), 7.16 – 7.12 (m, 1H), 7.07 (m, 2H), 7.02 (td, *J* = 8.8, 2.5 Hz, 1H), 3.77 (dd, *J* = 13.9, 6.3 Hz, 2H), 3.12 – 3.07 (m, 2H), 3.06 – 3.02 (m, 2H), 2.93 (t, *J* = 7.3 Hz, 2H), 2.81 (s, 3H). ^{13}C NMR (126 MHz, DMSO) δ 164.44, 163.37 (d, *J* = 243.2 Hz), 158.87, 143.12 (d, *J* = 7.4 Hz), 141.59, 139.72, 131.41 (d, *J* = 8.3 Hz), 129.54, 129.39, 127.28, 126.12, 126.10, 124.37, 116.64 (d, *J* = 14.6 Hz), 116.54, 114.25 (d, *J* = 20.8 Hz), 43.76, 38.43, 35.12, 33.58, 16.14. HRMS (ESI): calcd. 436.14950 for $C_{24}H_{23}FN_3O_2S$; found 436.1479 $[M+H]^+$.

4-((2-Fluorophenethyl)amino)-5-methyl-2-phenethylthieno[2,3-d]pyrimidine-6-carboxylic acid (26)

Isolated 21 mg (32% yield) as an off white powder. ^{1}H NMR (500 MHz, DMSO) δ 7.32 – 7.19 (m, 6H, NH), 7.12 (m, 3H), 3.76 (dd, *J* = 13.8, 6.7 Hz, 2H), 3.08 (m, 2H), 3.02 – 2.93 (m, 4H), 2.81 (s, 3H). ^{13}C NMR (126 MHz, DMSO) δ 164.90, 161.97 (d, *J* = 243.3 Hz),

159.18, 142.33, 139.88, 132.52 (d, J = 5.0 Hz), 129.59, 129.53, 129.47, 129.39, 127.10 (d, J = 16.1 Hz), 127.06, 125.55 (d, J = 3.3 Hz), 116.32 (d, J = 21.8 Hz), 116.16, 42.24, 34.08, 29.25, 16.34. HRMS (ESI): calcd. 436.14950 for $C_{24}H_{23}FN_3O_2S$; found 436.1476 $[M+H]^+$.

5-Methyl-4-((4-methylphenethyl)amino)-2-phenethylthieno[2,3-d]pyrimidine-6-carboxylic acid (27)

Isolated 48 mg (73% yield) as an off white powder. ^{1}H NMR (500 MHz, DMSO) δ 7.33 (m, NH), 7.26 – 7.21 (m, 4H), 7.16 – 7.09 (m, 5H), 3.72 (dd, J = 14.4, 6.2 Hz, 2H), 3.12 – 3.08 (m, 2H), 3.06 – 3.02 (m, 2H), 2.88 – 2.83 (m, 2H), 2.81 (s, 3H), 2.25 (s, 3H). ^{13}C NMR (126 MHz, DMSO) δ 164.64, 158.94, 141.90, 139.78, 137.16, 136.36, 130.15, 129.73, 129.52, 129.38, 127.19, 116.37, 44.09, 35.17, 33.81, 21.80, 16.25. HRMS (ESI): calcd. 432.17457 for $C_{25}H_{26}N_3O_2S$; found 432.1719 $[M+H]^+$.

5-Methyl-4-((3-methylphenethyl)amino)-2-phenethylthieno[2,3-d]pyrimidine-6-carboxylic acid (28)

Isolated 42 mg (64% yield) as an off white powder. ^{1}H NMR (500 MHz, DMSO) δ 7.45 (m, NH), 7.25 – 7.22 (m, 4H), 7.20 – 7.13 (m, 2H), 7.07 (s, 1H), 7.02 (m, 2H), 3.74 (dd, J = 14.6, 6.1 Hz, 2H), 3.12 (m, 2H), 3.06 (m, 2H), 2.89 – 2.84 (m, 2H), 2.81 (s, 3H), 2.25 (s, 3H). ^{13}C NMR (126 MHz, DMSO) δ 164.43, 158.82, 141.57, 140.02, 139.73, 138.61, 130.58, 129.56, 129.50, 129.38, 128.09, 127.30, 126.94, 116.59, 44.26, 38.35, 35.44, 33.55, 22.15, 16.12. HRMS (ESI): calcd. 432.17457 for $C_{25}H_{26}N_3O_2S$; found 432.1728 $[M+H]^+$.

5-Methyl-4-((2-methylphenethyl)amino)-2-phenethylthieno[2,3-d]pyrimidine-6-carboxylic acid (29)

Isolated 55 mg (84% yield) as an off white powder. ^{1}H NMR (500 MHz, DMSO) δ 7.42 (m, NH), 7.27 – 7.21 (m, 4H), 7.17 – 7.12 (m, 3H), 7.12 – 7.08 (m, 2H), 3.68 (dd, J = 15.5, 5.8 Hz, 2H), 3.11 – 3.06 (m, 2H), 3.04 – 2.99 (m, 2H), 2.93 – 2.88 (m, 2H), 2.85 (s, 3H), 2.40 (s, 3H). ^{13}C NMR (126 MHz, DMSO) δ 164.75, 159.07, 142.05, 139.79, 138.43, 137.20, 131.24, 130.55, 129.52, 129.33, 127.51, 127.16, 127.08, 116.25, 42.76, 34.25, 33.47, 20.10, 16.39. HRMS (ESI): calcd. 432.17457 for $C_{25}H_{26}N_3O_2S$; found 432.1746 $[M+H]^+$.

5-Methyl-2-phenethyl-4-((2-(pyridin-4-yl)ethyl)amino)thieno[2,3-d]pyrimidine-6-carboxylic acid (30)

Isolated 42 mg (64% yield) as a white powder. ^{1}H NMR (500 MHz, DMSO) δ 8.47 (d, J = 5.8 Hz, 2H), 7.28 (d, J = 5.7 Hz, 2H), 7.25 – 7.20 (m, 4H), 7.13 (m, NH, 1H), 3.77 (dd, J = 13.4, 6.6 Hz, 2H), 3.09 – 3.05 (m, 2H), 3.00 (m, 2H), 2.93 (t, J = 7.2 Hz, 2H), 2.80 (s, 3H). ^{13}C NMR (126 MHz, DMSO) δ 168.00, 167.89, 165.14, 159.23, 150.30, 142.65, 139.84, 129.42, 129.41, 126.95, 125.59, 122.11, 116.00, 42.20, 41.19, 35.03, 34.47, 16.48. HRMS (ESI): calcd. 419.15417 for $C_{23}H_{23}N_4O_2S$; found 419.1537 $[M+H]^+$.

5-Methyl-2-phenethyl-4-((2-(pyridin-3-yl)ethyl)amino)thieno[2,3-d]pyrimidine-6-carboxylic acid (31)

Isolated 41 mg (87% yield) as a white powder. ^{1}H NMR (500 MHz, DMSO) δ 8.45 (s, 1H), 8.40 (d, J = 4.7 Hz, 1H), 7.63 (d, J = 7.8 Hz, 1H), 7.30 (dd, J = 7.7, 4.8 Hz, 1H), 7.25 – 7.20

(m, 4H), 7.13 (m, 1H, NH), 3.75 (dd, *J* = 13.3, 6.7 Hz, 2H), 3.07 (dd, *J* = 8.4, 6.1 Hz, 2H), 2.99 (dd, *J* = 8.5, 6.3 Hz, 2H), 2.92 (t, *J* = 7.2 Hz, 2H), 2.80 (s, 3H). ^{13}C NMR (126 MHz, DMSO) δ 168.00, 167.89, 165.15, 159.25, 151.01, 148.56, 142.67, 139.82, 137.49, 136.22, 129.41, 126.94, 124.63, 122.11, 115.97, 42.86, 41.23, 34.49, 32.89, 16.47. HRMS (ESI): calcd. 419.15417 for $C_{23}H_{23}N_4O_2S$; found 419.1537 $[M+H]^+$.

5-Methyl-2-phenethyl-4-((2-(pyridin-2-yl)ethyl)amino)thieno[2,3-d]pyrimidine-6-carboxylic acid (32)

Isolated 57 mg (87% yield) as an off white solid. ^{1}H NMR (500 MHz, DMSO) δ 8.56 (d, *J* = 4.9 Hz, 1H), 7.83 (m, NH), 7.41 – 7.32 (m, 3H), 7.24 – 7.21 (m, 4H), 7.15 – 7.11 (m, 1H), 3.89 (dd, *J* = 12.4, 6.6 Hz, 2H), 3.12 (t, *J* = 6.7 Hz, 2H), 3.05 (m, 2H), 2.96 (m, 2H), 2.84 (s, 3H). ^{13}C NMR (126 MHz, DMSO) δ 167.80, 165.14, 159.92, 159.17, 148.62, 142.70, 139.82, 139.46, 129.42, 129.38, 126.90, 125.32, 123.35, 122.12, 115.99, 41.44, 41.17, 36.77, 34.40, 16.42. MS (ESI): calcd. 419.15417 for $C_{23}H_{23}N_4O_2S$; found 419.1545 $[M+H]^+$

2-(4-Acetamidophenethyl)-5-methyl-4-(methylamino)thieno[2,3-d]pyrimidine-6-carboxylic acid (33)

Isolated 27 mg (72% yield) as an off white powder. ^{1}H NMR (500 MHz, DMSO) δ 9.85 (s, NHAc), 7.46 (m, NH), 7.44 (d, *J* = 8.3 Hz, 2H), 7.15 (d, *J* = 8.3 Hz, 2H), 3.03 (m, 7H), 2.87 (s, 3H), 1.99 (s, 3H). ^{13}C NMR (126 MHz, DMSO) δ 169.25, 164.47, 159.15, 139.96, 138.66, 136.03, 129.62, 124.20, 120.16, 116.72, 38.55, 33.04, 30.12, 25.10, 16.22. HRMS (ESI): calcd. 385.13344 for $C_{19}H_{21}N_4O_3S$; found 385.1336 $[M+H]^+$.

2-(3-Acetamidophenethyl)-5-methyl-4-(methylamino)thieno[2,3-d]pyrimidine-6-carboxylic acid (34)

Isolated 23 mg (62% yield) as a white powder. ^{1}H NMR (500 MHz, DMSO) δ 9.84 (s, NHAc), 7.47 (s, 1H), 7.37 (d, *J* = 8.3 Hz, 1H), 7.15 (t, *J* = 7.8 Hz, 1H), 7.08 (m, NH), 6.90 (d, *J* = 7.9 Hz, 1H), 3.05 – 2.94 (m, 7H), 2.86 (s, 3H), 2.00 (s, 3H). ^{13}C NMR (126 MHz, DMSO) δ 169.33, 167.60, 165.14, 159.80, 143.12, 140.46, 140.07, 129.69, 124.16, 121.93, 120.00, 117.75, 116.19, 34.57, 29.33, 25.18, 16.55. HRMS (ESI): calcd. 385.13344 for $C_{19}H_{21}N_4O_3S$; found 385.1333 $[M+H]^+$.

2-(2-Acetamidophenethyl)-5-methyl-4-(methylamino)thieno[2,3-d]pyrimidine-6-carboxylic acid (35)

Isolated 13 mg (46% yield) as an off white powder. ^{1}H NMR (500 MHz, DMSO) δ 9.40 (s, NHAc), 7.32 (d, *J* = 7.8 Hz, 1H), 7.25 (d, *J* = 7.6 Hz, 1H), 7.14 (m, NH), 7.08 (m, 2H), 3.08 – 3.02 (m, 2H), 2.98 (d, *J* = 4.4 Hz, 3H), 2.96 – 2.91 (m, 2H), 2.86 (s, 3H), 2.04 (s, 3H). ^{13}C NMR (126 MHz, DMSO) δ 169.54, 168.12, 165.17, 159.83, 140.10, 137.22, 136.98, 130.26, 127.28, 126.57, 121.82, 116.18, 30.04, 29.25, 24.42, 16.58. HRMS (ESI): calcd. 385.13344 for $C_{19}H_{21}N_4O_3S$; found 385.1331 $[M+H]^+$.

4-((2,3-Dihydro-1H-inden-2-yl)amino)-5-methyl-2-phenethylthieno[2,3-d]pyrimidine-6-carboxylic acid (36)

Isolated 47 mg (72% yield) as an off white powder. ^{1}H NMR (500 MHz, DMSO) δ 7.25 – 7.19 (m, 5H, NH), 7.17 – 7.12 (m, 3H), 6.91 (d, *J* = 7.0 Hz, 1H), 5.07 – 4.98 (m, 1H), 3.36 – 3.28 (m, 2H), 3.09 – 3.04 (m, 3H), 3.01 (m, 3H), 2.87 (s, 3H). ^{13}C NMR (126 MHz, DMSO) δ 168.05, 167.84, 165.15, 159.46, 142.65, 142.33, 140.06, 129.41, 129.37, 127.58, 126.91, 125.53, 122.21, 116.24, 53.03, 41.21, 39.86, 34.49, 16.39. HRMS (ESI): calcd. 430.15892 for $C_{25}H_{24}N_3O_2S$; found 430.1562 $[M+H]^+$.

4-((3,5-Dimethoxyphenethyl)amino)-5-methyl-2-phenethylthieno[2,3-d]pyrimidine-6-carboxylic acid (37)

Isolated 31 mg (82% yield) as an off white powder. ^{1}H NMR (500 MHz, DMSO) δ 7.24 – 7.22 (m, 4H), 7.16 – 7.09 (m, 1H, NH), 6.41 (d, *J* = 2.2 Hz, 2H), 6.33 (t, *J* = 2.2 Hz, 1H), 3.73 (dd, *J* = 14.5, 6.4 Hz, 2H), 3.67 (s, 6H), 3.10 (m, 2H), 3.01 (m, 2H), 2.87 – 2.82 (m, 2H), 2.81 (s, 3H). ^{13}C NMR (126 MHz, DMSO) δ 165.08, 161.61, 159.21, 142.94, 142.57, 139.84, 129.42, 129.38, 126.99, 116.05, 107.83, 99.15, 56.13, 43.42, 36.02, 34.40, 16.41. MS (ESI): calcd. 478.18005 for $C_{26}H_{28}N_3O_4S$; found 478.1782 $[M+H]^+$.

4-((2-(Benzo[d][1,3]dioxol-5-yl)ethyl)amino)-5-methyl-2-phenethylthieno[2,3-d]pyrimidine-6-carboxylic acid (38)

Isolated 22 mg (47% yield) as a white solid. ^{1}H NMR (500 MHz, DMSO) δ 7.27 – 7.18 (m, 5H, NH), 7.16 – 7.12 (m, 1H), 6.82 (m, 2H), 6.68 (dd, *J* = 7.9, 1.6 Hz, 1H), 5.95 (s, 2H), 3.70 (dd, *J* = 14.0, 6.0 Hz, 1H), 3.13 – 3.06 (m, 2H), 3.02 (m, 2H), 2.85 – 2.78 (m, 5H). ^{13}C NMR (126 MHz, DMSO) δ 164.83, 159.07, 148.43, 146.76, 142.18, 139.85, 134.16, 129.49, 129.40, 127.12, 122.76, 116.24, 110.19, 109.33, 101.86, 43.92, 35.33, 34.07, 16.31. HRMS (ESI): calcd. 462.14875 for $C_{25}H_{24}N_3O_4S$; found 462.1486 $[M+H]^+$.

5-Methyl-4-(methylamino)-2-(3-phenylpropyl)thieno[2,3-d]pyrimidine-6-carboxylic acid (39)

Isolated 36 mg (78% yield) as a white powder. ^{1}H NMR (500 MHz, DMSO) δ 7.25 (m, 2H), 7.19 (m, 2H), 7.14 (m, 1H, NH), 2.97 (d, *J* = 4.4 Hz, 3H), 2.84 (s, 3H), 2.69 (t, *J* = 7.5 Hz, 2H), 2.62 (t, *J* = 7.6 Hz, 2H), 2.05 – 1.97 (m, 2H). ^{13}C NMR (126 MHz, DMSO) δ 168.13, 165.10, 159.76, 143.09, 140.03, 129.53, 129.38, 126.84, 121.96, 116.11, 38.83, 35.90, 30.49, 29.34, 16.50. MS (ESI): calcd 342.12762 for $C_{18}H_{20}N_3O_2S$; found 342.1256 $[M+H]^+$.

5-Methyl-4-(methylamino)-2-(4-phenylbutyl)thieno[2,3-d]pyrimidine-6-carboxylic acid (40)

Isolated 60 mg (86% yield) as white powder. ^{1}H NMR (500 MHz, DMSO) δ 7.23 (t, *J* = 7.5 Hz, 2H), 7.13 (m, 3H), 7.03 (br. m, NH), 2.94 (d, *J* = 4.4 Hz, 3H), 2.84 (s, 3H), 2.69 (t, *J* = 7.5 Hz, 2H), 2.58 (t, *J* = 7.6 Hz, 2H), 1.76 – 1.68 (m, 2H), 1.63 – 1.55 (m, 2H). ^{13}C NMR (126 MHz, DMSO) δ 168.72, 167.39, 165.17, 159.83, 143.33, 140.06, 129.42, 129.34, 126.74, 121.71, 116.03, 39.49, 36.12, 31.86, 29.21, 28.41, 16.53. HRMS (ESI): calcd 356.14327 for $C_{19}H_{22}N_3O_2S$; found 356.1413 $[M+H]^+$.

2-(3-Methoxyphenethyl)-5-methyl-4-(methylamino)thieno[2,3-d]pyrimidine-6-carboxylic acid (41)

Isolated 66 mg (71% yield) as a white powder. ^{1}H NMR (500 MHz, DMSO) δ 7.12 (t, *J* = 8.0 Hz, 1H), 7.01 (m, NH), 6.77 (m, 2H), 6.68 (dd, *J* = 9.0, 1.6 Hz, 1H), 3.05 – 2.93 (m, 7H), 2.82 (s, 3H). OC*H*$_3$ signal obscured by water peak. ^{13}C NMR (126 MHz, DMSO) δ 167.90, 167.48, 165.15, 160.29, 159.80, 144.29, 140.03, 130.39, 121.82, 121.70, 116.09, 115.03, 112.39, 55.95, 41.03, 34.37, 29.19, 16.48. MS (ESI): calc. 358.12254 for $C_{18}H_{20}N_3O_3S$; found 358.1208 $[M+H]^+$.

2-(3-Fluorophenethyl)-5-methyl-4-(methylamino)thieno[2,3-d]pyrimidine-6-carboxylic acid (42)

Isolated 77 mg (83% yield) as a white powder. ^{1}H NMR (500 MHz, DMSO) δ 7.24 (m, 1H), 7.02 (m, 2H, NH), 6.93 (m, 1H), 3.06 (t, *J* = 7.5 Hz, 2H), 3.00 – 2.95 (m, 2H), 2.94 (d, *J* = 4.5 Hz, 3H), 2.81 (s, 3H). ^{13}C NMR (126 MHz, DMSO) δ 167.64, 167.50, 165.14, 163.28 (d, J = 242.8 Hz), 159.77, 145.69 (d, J = 7.3 Hz), 140.01, 131.16 (d, J = 8.4 Hz), 125.58 (d, J = 2.6 Hz), 121.85, 116.12 (d, J = 20.7 Hz), 116.09, 113.65 (d, J = 20.9 Hz), 40.65, 33.89, 29.17, 16.47. HRMS (ESI): calcd. 346.10255 for $C_{17}H_{17}FN_3O_2S$; found 346.1006 $[M+H]^+$.

5-Methyl-4-(methylamino)-2-(2-(pyridin-2-yl)ethyl)thieno[2,3-d]pyrimidine-6-carboxylic acid (43)

Isolated 46 mg (84% yield) as a white powder. ^{1}H NMR (300 MHz, DMSO) δ 8.75 (d, *J* = 4.9 Hz, 1H), 8.41 (td, *J* = 7.9, 1.5 Hz, 1H), 7.95 (d, *J* = 8.0 Hz, 1H), 7.82 (t, *J* = 6.3 Hz, 1H), 7.17 (br. m, NH), 3.47 (t, *J* = 7.1 Hz, 2H), 3.27 (t, *J* = 7.1 Hz, 2H), 2.80 (m, 6H). ^{13}C NMR (75 MHz, DMSO) δ 165.80, 165.33, 164.51, 159.13, 157.64, 146.10, 142.19, 139.47, 127.38, 125.11, 121.94, 115.76, 36.57, 31.33, 28.73, 15.89. HRMS (ESI): calcd. 329.10722 for $C_{16}H_{17}N_4O_2S$; found 329.1067 $[M+H]^+$.

2-(4-Acetamidophenethyl)-4-((2-aminoethyl)amino)-5-methylthieno[2,3-d]pyrimidine-6-carboxylic acid (44)

Isolated 17 mg (36% yield) as a white powder. ^{1}H NMR (500 MHz, DMSO) δ 9.84 (s, NHAc), 8.50 (br. s, NH_2), 7.56 (br. s, NH), 7.44 (d, *J* = 8.3 Hz, 2H), 7.15 (d, *J* = 8.4 Hz, 2H), 3.82 (m, 2H), 3.15 (m, 2H), 3.03 (s, 3H), 3.00 (d, *J* = 7.2 Hz, 2H), 2.94 (d, *J* = 7.8 Hz, 2H), 2.00 (s, 3H). HRMS (ESI): calcd. 414.15999 for $C_{20}H_{24}N_5O_3S$; found 414.1591 $[M+H]^+$.

2-(4-Acetamidophenethyl)-5-methyl-4-((2-(pyridin-2-yl)ethyl)amino)thieno[2,3-d]pyrimidine-6-carboxylic acid (45)

Isolated 33 mg (64% yield) as a white powder. ^{1}H NMR (500 MHz, DMSO) δ 9.83 (s, NH), 8.51 (d, *J* = 4.9 Hz, 1H), 7.71 (tt, *J* = 7.7, 1.9 Hz, 1H), 7.42 (d, *J* = 6.8 Hz, 2H), 7.36 (br. t, *J* = 4.8 Hz, NH), 7.28 (d, *J* = 7.8 Hz, 1H), 7.25 – 7.20 (m, 1H), 7.13 (d, *J* = 6.9 Hz, 2H), 3.87 (dd, *J* = 12.2, 5.5 Hz, 2H), 3.08 (t, *J* = 6.5 Hz, 2H), 3.04 – 2.99 (m, 2H), 2.97 – 2.93 (m, 2H), 2.85 (s, 3H), 1.99 (s, 3H). ^{13}C NMR (126 MHz, DMSO) δ 169.20, 167.80, 165.22, 160.73, 159.22, 150.13, 138.30, 137.87, 137.25, 129.57, 124.49, 122.79, 120.13, 116.03, 41.56,

41.31, 37.42, 33.89, 25.07, 16.32. HRMS (ESI): calcd. 476.17564 for $C_{25}H_{26}N_5O_3S$; found 476.1761 $[M+H]^+$

2-(3-Chlorophenethyl)-5-methyl-4-(methylamino)thieno[2,3-d]pyrimidine-6-carboxylic acid (46)

Isolated 62 mg (67% yield) as a white powder. ^{1}H NMR (500 MHz, DMSO) δ 7.28 (s, 1H), 7.25 – 7.21 (m, 1H), 7.18 – 7.14 (m, 2H), 7.03 (m, NH), 3.07 – 3.02 (m, 2H), 2.97 (m, 2H), 2.94 (d, *J* = 4.5 Hz, 3H), 2.81 (s, 3H). ^{13}C NMR (126 MHz, DMSO) δ 167.47, 167.21, 165.11, 159.74, 145.25, 140.00, 133.93, 131.16, 129.37, 128.21, 126.90, 121.93, 116.10, 40.51, 33.75, 29.20, 16.46. HRMS (ESI): calcd. 362.07300 for $C_{17}H_{17}ClN_3O_2S$; found 362.0719 $[M+H]^+$.

5-Methyl-4-(methylamino)-2-(3-(trifluoromethyl)phenethyl)thieno[2,3-d]pyrimidine-6-carboxylic acid (47)

Isolated 80 mg (86% yield) as a white powder. ^{1}H NMR (500 MHz, DMSO) δ 7.55 (s, 1H), 7.46 (m, 3H), 7.04 (br. m, NH), 3.14 (t, *J* = 7.5 Hz, 2H), 3.02 (t, *J* = 7.5 Hz, 2H), 2.92 (d, *J* = 4.4 Hz, 3H), 2.81 (s, 3H). ^{13}C NMR (126 MHz, DMSO) δ 167.36, 167.13, 165.10, 159.73, 144.05, 139.97, 133.66, 130.31, 130.16, 129.91, δ 126.06 (q, *J* = 3.8 Hz), 123.66 (q, *J* = 3.9 Hz), 121.96, 116.09, 33.79, 29.14, 16.44. HRMS (ESI): calcd. 396.09936 for $C_{18}H_{17}F_3N_3O_2S$; found 396.0975 $[M+H]^+$.

2-(2-(Benzo[d][1,3]dioxol-5-yl)ethyl)-5-methyl-4-(methylamino)thieno[2,3-d]pyrimidine-6-carboxylic acid (48)

Isolated 25 mg (54% yield) as white solid. ^{1}H NMR (500 MHz, DMSO) δ 7.13 (br. s, NH), 6.82 (s, 1H), 6.77 (d, *J* = 7.9 Hz, 1H), 6.67 (d, *J* = 7.9 Hz, 1H), 5.93 (s, 2H), 3.02 – 2.93 (m, 7H), 2.86 (s, 3H). ^{13}C NMR (126 MHz, DMSO) δ 167.45, 165.09, 159.73, 148.25, 146.39, 140.07, 136.42, 122.21, 122.05, 116.18, 109.95, 109.18, 101.72, 41.21, 34.01, 29.36, 16.53. HRMS (ESI): calcd. 372.10180 for $C_{18}H_{18}N_3O_4S$; found 372.1021 $[M+H]^+$.

4-(methylamino)-2-phenethylthieno[3,2-d]pyrimidine-6-carboxylic acid (49)

Isolated 40 mg (84% yield) as an off-white powder. ^{1}H NMR (500 MHz, DMSO) δ 7.99 (m, NH), 7.81 (s, 1H), 7.27 – 7.23 (m, 4H), 7.16 (m, 1H), 3.12 – 3.07 (m, 2H), 3.05 – 3.01 (m, 2H), 2.99 (d, *J* = 4.0 Hz, 3H). ^{13}C NMR (126 MHz, DMSO) δ 167.38, 164.21, 158.49, 142.88, 130.23, 129.48, 129.39, 126.90, 41.32, 34.82, 28.44. HRMS (ESI): calcd. 314.09632 for $C_{16}H_{16}N_3O_2S$; found 314.0962 $[M+H]^+$.

2-(3-Methoxyphenethyl)-4-(methylamino)thieno[3,2-d]pyrimidine-6-carboxylic acid (50)

Isolated 78 mg (81% yield) as a white powder. ^{1}H NMR (500 MHz, DMSO) δ 8.11 (br. d, *J* = 4.3 Hz, 1H), 7.76 (s, 1H), 7.13 (t, *J* = 7.8 Hz, 1H), 6.81 – 6.75 (m, 2H), 6.68 (dd, *J* = 8.3, 1.7 Hz, 1H), 3.04 – 2.99 (m, 4H), 2.97 (d, *J* = 4.4 Hz, 3H). OC*H*$_3$ signal obscured by water peak. ^{13}C NMR (126 MHz, DMSO) δ 167.10, 164.14, 160.30, 144.29, 130.40, 129.32, 121.72, 121.68, 115.03, 112.40, 55.95, 40.79, 34.69. HRMS (ESI): calcd. 344.10689 for $C_{17}H_{18}N_3O_3S$; found 344.1072 $[M+H]^+$.

Ethyl 4-(((R)-2-methoxy-2-phenylethyl)amino)-5-methyl-2-((S)-2-phenylpropyl)thieno[2,3-d]pyrimidine-6-carboxylate – 51 (precursor)

Isolated 101 mg (53% yield) as a colorless syrup. ^{1}H NMR (500 MHz, DMSO) δ 7.38 (m, 2H), 7.34 – 7.28 (m,), 7.22 (m, 5H), 7.10 (t, *J* = 6.8 Hz, 1H), 6.96 (br. t, *J* = 5.5 Hz, NH), 4.54 (dd, *J* = 7.5, 5.3 Hz, 1H), 4.27 (q, *J* = 7.1 Hz, 2H), 3.76 – 3.69 (m, 1H), 3.69 – 3.61 (m, 1H), 3.43 (m, 1H), 3.18 (s, 3H), 2.96 (m, 2H), 2.76 (s, 3H), 1.28 (t, *J* = 7.1 Hz, 3H), 1.20 (d, *J* = 6.9 Hz, 3H). ^{13}C NMR (75 MHz, DMSO) δ 167.65, 167.15, 162.87, 158.58, 147.31, 140.51, 140.03, 129.07, 128.85, 128.46, 127.41, 127.19, 126.50, 120.06, 115.15, 81.57, 79.84, 61.61, 57.16, 47.51, 39.04, 22.62, 15.94, 14.75. MS (ESI): calcd. 490.22; found 490.33 $[M+H]^{+}$.

4-(((R)-2-methoxy-2-phenylethyl)amino)-5-methyl-2-((S)-2-phenylpropyl)thieno[2,3-d]pyrimidine-6-carboxylic acid (51)

Isolated 13 mg (28% yield) as white solid. ^{1}H NMR (500 MHz, DMSO) δ 7.38 (m, 2H), 7.31 (m, 3H), 7.22 (m, 4H), 7.12 – 7.08 (m, 1H), 6.85 (br. s, NH), 4.54 (m, 1H), 3.72 (m, 1H), 3.68 – 3.60 (m, 1H), 3.18 (s, 3H), 3.02 – 2.86 (m, 3H), 2.75 (s, 3H), 1.20 (d, *J* = 6.9 Hz, 3H). ^{13}C NMR (126 MHz, DMSO) δ 167.68, 167.10, 165.30, 159.07, 147.85, 141.06, 129.60, 129.40, 128.99, 127.97, 127.75, 127.04, 115.94, 82.06, 57.70, 47.98, 47.61, 39.57, 23.21, 16.17. HRMS (ESI): calcd. 462.18514 for $C_{26}H_{28}N_3O_3S$; found 462.1853 $[M+H]^{+}$

Ethyl 4-(((S)-2-methoxy-2-phenylethyl)amino)-5-methyl-2-((S)-2-phenylpropyl)thieno[2,3-d]pyrimidine-6-carboxylate 52 (precursor)

Isolated 31 mg (16% yield) as a colorless syrup. ^{1}H NMR (500 MHz, DMSO) δ 7.41 – 7.36 (m, 2H), 7.31 (m, 3H), 7.25 – 7.20 (m, 4H), 7.10 (m, 1H), 6.99 (br. t, *J* = 5.4 Hz, NH), 4.51 (dd, *J* = 7.8, 4.7 Hz, 1H), 4.27 (q, *J* = 7.1 Hz, 2H), 3.79 – 3.73 (m, 1H), 3.62 (m, 1H), 3.44 (m, 1H), 3.17 (s, 3H), 2.95 (m, 2H), 2.78 (s, 3H), 1.28 (t, *J* = 7.1 Hz, 3H), 1.22 (d, *J* = 7.0 Hz, 3H). ^{13}C NMR (75 MHz, DMSO) δ 167.62, 167.17, 162.90, 158.60, 147.27, 140.52, 140.12, 129.11, 128.88, 128.51, 127.45, 127.20, 126.54, 120.05, 115.17, 81.63, 61.68, 57.21, 47.49, 36.87, 24.96, 22.71, 16.00, 14.80. MS (ESI): calcd. 490.22; found 490.40 $[M+H]^{+}$.

4-(((S)-2-Methoxy-2-phenylethyl)amino)-5-methyl-2-((S)-2-phenylpropyl)thieno[2,3-d]pyrimidine-6-carboxylic acid (52)

Isolated 15 mg (53% yield) as a white solid. ^{1}H NMR (500 MHz, DMSO) δ 7.39 (m, 2H), 7.31 (m, 3H), 7.21 (m, 4H), 7.10 (m, 1H), 6.97 (m, NH), 4.51 (dd, *J* = 7.7, 4.4 Hz, 1H), 3.76 (m, 1H), 3.62 (m, 1H), 3.17 (s, 3H), 2.95 (m, 3H), 2.77 (s, 3H), 1.22 (d, *J* = 6.9 Hz, 3H). ^{13}C NMR (126 MHz, DMSO) δ 167.30, 165.07, 159.10, 147.75, 141.02, 139.64, 129.62, 129.40, 129.02, 127.97, 127.73, 127.07, 122.30, 115.88, 82.12, 57.72, 47.89, 47.70, 39.49, 23.24, 16.32. HRMS (ESI): calcd. 462.18514 for $C_{26}H_{28}N_3O_3S$; found 462.1857 $[M+H]^{+}$.

Ethyl 4-(((R)-2-methoxy-2-phenylethyl)amino)-5-methyl-2-((R)-2-phenylpropyl)thieno[2,3-d]pyrimidine-6-carboxylate 53 (precursor)

Isolated 65 mg (63% yield) as pale yellow syrup. ^{1}H NMR (300 MHz, $CDCl_3$) δ 7.46 – 7.20 (m, 9H), 7.16 – 7.09 (m, 1H), 6.11 (br. t, NH), 4.41 – 4.31 (m, 3H), 4.08 (ddd, *J* = 13.8, 7.2,

4.0 Hz, 1H), 3.56 – 3.44 (m, 2H), 3.30 (s, 3H), 3.17 – 2.96 (m, 2H), 2.87 (s, 3H), 1.39 (t, *J* = 7.1 Hz, 3H), 1.29 (d, *J* = 7.0 Hz, 3H). ^{13}C NMR (75 MHz, $CDCl_3$) δ 163.33, 158.77, 147.18, 139.30, 138.36, 128.97, 128.57, 128.47, 127.27, 126.87, 126.13, 115.37, 82.07, 61.45, 57.25, 47.11, 39.30, 24.96, 22.09, 15.71, 14.56. MS (ESI): calcd. 490.22; found 490.33 $[M+H]^+$.

4-(((R)-2-Methoxy-2-phenylethyl)amino)-5-methyl-2-((R)-2-phenylpropyl)thieno[2,3-d]pyrimidine-6-carboxylic acid (53)

Isolated 43 mg (76% yield) as white solid. ^{1}H NMR (500 MHz, DMSO) δ 7.39 (m, 2H), 7.31 (m, 3H), 7.25 – 7.18 (m, 4H), 7.12 – 7.07 (m, 1H), 7.04 (br. t, *J* = 5.4 Hz, NH), 4.50 (dd, *J* = 7.9, 4.7 Hz, 1H), 3.80 – 3.73 (m, 1H), 3.66 – 3.61 (m, 1H), 3.17 (s, 3H), 2.96 (m, 4H), 2.77 (s, 3H), 1.22 (d, *J* = 7.0 Hz, 3H). ^{13}C NMR (126 MHz, DMSO) δ 167.06, 165.01, 159.08, 147.65, 140.95, 139.63, 129.63, 129.42, 129.04, 127.96, 127.73, 127.10, 122.47, 115.92, 82.10, 68.17, 57.72, 47.73, 39.47, 23.22, 16.28. HRMS (ESI): calcd. 462.18514 for $C_{26}H_{28}N_3O_3S$; found 462.1847 $[M+H]^+$.

Ethyl 4-(((S)-2-methoxy-2-phenylethyl)amino)-5-methyl-2-((R)-2-phenylpropyl)thieno[2,3-d]pyrimidine-6-carboxylate 54 (precursor)

Isolated 67 mg (65% yield) as a colorless syrup. ^{1}H NMR (300 MHz, $CDCl_3$) δ 7.46 – 7.32 (m, 5H), 7.30 – 7.19 (m, 4H), 7.13 (dt, *J* = 9.3, 4.2 Hz, 1H), 6.11 (br. t, NH), 4.39 (m, 3H), 4.06 (ddd, *J* = 13.7, 7.0, 4.1 Hz, 1H), 3.57 – 3.44 (m, 2H), 3.31 (s, 3H), 3.08 (m, 2H), 2.87 (s, 3H), 1.38 (t, *J* = 6.2 Hz, 3H), 1.27 (d, *J* = 6.9 Hz, 3H). ^{13}C NMR (75 MHz, $CDCl_3$) δ 163.33, 158.78, 147.22, 139.29, 138.35, 128.97, 128.57, 128.47, 127.26, 126.88, 126.12, 115.37, 82.06, 61.45, 57.24, 47.06, 39.28, 36.93, 22.18, 15.68, 14.55. MS (ESI): calcd. 490.22; found 490.33 $[M+H]^+$.

4-(((S)-2-Methoxy-2-phenylethyl)amino)-5-methyl-2-((R)-2-phenylpropyl)thieno[2,3-d]pyrimidine-6-carboxylic acid (54)

Isolated 42 mg (74% yield) as a yellow solid. ^{1}H NMR (500 MHz, DMSO) δ 7.41 – 7.36 (m, 2H), 7.34 – 7.29 (m, 3H), 7.26 – 7.19 (m, 4H), 7.12 – 7.08 (m, 1H), 7.00 (br. t, *J* = 5.5 Hz, NH), 4.54 (dd, *J* = 7.6, 5.1 Hz, 1H), 3.76 – 3.70 (m, 1H), 3.69 – 3.62 (m, 1H), 3.18 (s, 3H), 2.96 (m, 3H), 2.75 (s, 3H), 1.20 (d, *J* = 7.0 Hz, 3H). ^{13}C NMR (126 MHz, DMSO) δ 167.12, 165.02, 159.09, 147.68, 140.96, 139.62, 129.62, 129.43, 129.04, 127.96, 127.75, 127.10, 122.45, 115.91, 82.02, 68.17, 57.70, 47.71, 39.55, 23.20, 16.25. HRMS (ESI): calcd. 462.18514 for $C_{26}H_{28}N_3O_3S$; found 462.1847 $[M+H]^+$.

Ethyl (S)-2-(4-acetamidophenethyl)-4-((2-methoxy-2-phenylethyl)amino)-5-methylthieno[2,3-d]pyrimidine-6-carboxylate 55 (precursor)

Isolated 40 mg (82% yield, over two steps) as a white powder. ^{1}H NMR (300 MHz, $CDCl_3$) δ 7.55 (s, 1H), 7.41 (m, 7H), 7.15 (d, *J* = 8.4 Hz, 2H), 6.16 (br. m, NH), 4.43 (dd, *J* = 8.6, 3.8 Hz, 1H), 4.34 (q, *J* = 7.1 Hz, 2H), 4.14 (ddd, *J* = 14.0, 7.0, 4.3 Hz, 1H), 3.54 (ddd, *J* = 13.7, 8.7, 3.8 Hz, 1H), 3.31 (s, 3H), 3.07 (m, 4H), 2.88 (s, 3H), 2.12 (s, 3H), 1.38 (t, *J* = 7.1 Hz, 4H). ^{13}C NMR (75 MHz, $CDCl_3$) δ 163.32, 158.91, 150.73, 137.95, 129.11, 128.98,

126.87, 120.18, 115.46, 84.48, 61.49, 57.24, 47.08, 41.08, 33.87, 24.72, 15.72, 14.55. MS (ESI): calcd. 533.22; found 533.27$[M+H]^+$.

(S)-2-(4-Acetamidophenethyl)-4-((2-methoxy-2-phenylethyl)amino)-5-methylthieno[2,3-d]pyrimidine-6-carboxylic acid (55)

Isolated 24 mg (63% yield) as a white powder. ^{1}H NMR (500 MHz, DMSO) δ 9.81 (s, NHAc), 7.43 (d, *J* = 8.5 Hz, 2H), 7.39 – 7.28 (m, 5H), 7.12 (d, *J* = 8.5 Hz, 2H), 6.98 (br. t, *J* = 5.2 Hz, NH), 4.54 (dd, *J* = 7.7, 5.0 Hz, 1H), 3.80 (m, 1H), 3.67 (m, 1H), 3.18 (s, 3H), 2.98 (m, 4H), 2.79 (s, 3H), 1.98 (s, 3H). ^{13}C NMR (126 MHz, DMSO) δ 169.15, 167.82, 165.09, 159.21, 141.02, 139.66, 138.37, 137.11, 129.61, 129.55, 129.00, 127.75, 122.32, 120.10, 115.96, 82.14, 57.69, 47.66, 41.28, 33.91, 25.08, 16.33. HRMS (ESI): calcd. 505.19095 for $C_{27}H_{29}N_4O_4S$; found 505.1916 $[M+H]^+$.

Protein expression and purification

The heterologous expression of PglD was accomplished using the *E. coli* BL-21(DE3) strain (Stratagene). Cells were transformed with pETNO-construct plasmids and grown to an A600 of 0.6 absorbance units at 37 °C in Lysogeny broth; the cultures were cooled to 16 °C and then induced by the addition of 0.5 mM isopropyl-D-thiogalactopyranoside (IPTG). The pETNO plasmid is based on the pET30a plasmid modified to include a His_8TEV (purification tag/protease cleavage site) in place of the existing His_6-thrombin site. Twenty hours after induction the cells were harvested by centrifugation and resuspended in ice-cold buffer composed of 50 mM HEPES pH 7.1, 10 mM imidazole, 150 mM NaCl, at1/20 the original culture volume. Maintaining a working temperature of 4 °C, the cells were lysed by sonication, and the lysate was cleared by centrifugation in a Type 45 Ti rotor (Beckman/Coulter) at 35,000 rpm. The extract was bound to Ni-NTA (Qiagen) in batch mode using 1 mL of resin per liter of culture for 1h with gentle tumbling. The protein-bound resin was washed with 25 column volumes of lysis buffer containing 50 mM imidazole, and the protein was eluted in lysis buffer containing 250 mM imidazole. The hexahistidine tag was removed by TEV cleavage, and after the digest reached completion, the reaction was dialyzed twice against 4 L 20 mM HEPES pH 7.1, 150 mM NaCl with a 10,000 MWCO Snakeskin (Thermo Scientific). Further purification was performed by size exclusion chromatography using a Superdex 200 XK16–60 column (GE Healthcare) in a running buffer of 20 mM HEPES pH 7.1, 100 mM NaCl.

High-throughput screening – Broad Institute MLPCN

To a Nunc 384-well black-clear bottom plate (Thermo Scientific) was added 200 nL of compound in neat DMSO (final assay concentration = 10 μM) and 20 μL of enzyme solution (final assay concentrations: 6 nM PglD, 50 mM HEPES pH 7.4, 0.001% Triton, 0.05% BSA, 100 μM AcCoA). Solution dispensing was accomplished utilizing a Multidrop Combi (Thermo Scientific). This mixture was allowed to incubate at room temperature for a duration of 45 minutes. The reaction was started by the addition of 10 μL reaction solution (final assay concentrations: 50 mM HEPES pH7.4, 100 μM UDP-4-aminosugar). The reaction was quenched after 30 minutes with the addition of 30 μL stop solution (final assay concentrations: 2 mM DTNB, 1 mM EDTA, 20% 1-propanol). The plates were allowed to develop for 5 minutes before reading at a λ = 405 nm.

Enzymatic inhibition assay

Kinetic characterization of PglD inhibition was carried out by monitoring CoASH release resulting from the acetyltransferase reaction with Ellman's reagent (DTNB) in a continuous fashion. To a flat, clear bottom 96-well plate (Falcon) was added sequentially the inhibitor as a DMSO stock solution, followed by PglD in 50 mM HEPES pH 7.8, 1 mM $MgCl_2$, 0.05 mg/mL BSA, 0.001% Triton X-100. Inhibitors and enzyme were pre-incubated 30 min at RT, followed by addition of substrate and Ellman's reagent cocktail to final concentrations of 3 nM PglD, 500 μM 4-amino-sugar, 300 μM AcCoA, 2 mM DTNB and 3% DMSO in 150 μL volume. Initial rates were measured in the linear portion of the reaction curve over a 5 min time period at RT, measuring absorbance at 412 nm on a Synergy H1 hybrid plate reader from Biotek.

Dynamic Light Scattering

Samples were prepared in buffer 50 mM HEPES 7.5, 100 mM NaCl and a final concentration of 3% DMSO; the concentration of *C jejuni* PglD was 25 μM with or without 250 μM inhibitor **57**. DLS data was acquired on a Wyatt DynaPro Nanostar Light Scatterer by measuring scattering at a 90° angle with a 685 nm laser and analyzed with a Rayleigh scattering model using the Dynamics 7.1.9 software package.

Differential Scanning Fluorimetry

Samples were prepared to a final volume of 25 μL containing 10 μM PglD protein and 100 μM inhibitor in a buffer containing 50 mM HEPES 7.5, 150 mM NaCl, 0.001 % Triton X-100, 10× Sypro orange (diluted from a commercial stock solution of 5000X; Invitrogen) and a final concentration of 3% DMSO. All samples were prepared in duplicate. Fluorescence was measured using a Roche Lightcycler 480 RT-PCR instrument while increasing the temperature gradient from 30 to 95°C in increments of 4.4°C/60 s. The midpoint temperature of the unfolding protein transition (T_m) was calculated using the built-in functionality of the instrument software package.

Crystallization of C. jejuni PglD in complex with inhibitor 17

Initial crystallization screening was performed by sitting drop vapor diffusion using intelli-plate® from Hampton Research with 50 μL/well solution, which was dispensed as a 0.15 μL drop followed 0.15 μL of 10 mg/mL PglD solution in SEC buffer. Screens used were PEG suite 1, PEG suite 2, PACT and ProComp from Qiagen, and drops were set up using an Art Robbins Phoenix robot. Diffraction quality crystals were formed via hanging drop vapor diffusion by mixing 1.5 μL of protein solution with 1.5 μL of reservoir solution (15% PEG-3350, 0.1M NaF and 10% glycerol) and incubation at 22 °C.

Ligand soaking: Wells were carefully opened and 50 μL of DMSO was added directly to the well; 0.75 μL of a solution containing 10 mM inhibitor **17** in reservoir solution (final concentration of 10% DMSO) was added directly to the drops on the slide. The crystals were then incubated for 30 min to 3 days, and then looped and flash frozen in liquid nitrogen without the need of separate cryoprotection.

Data Collection, Processing, and Structure Refinement

Diffraction data was collected either at a home source (Rigaku Saturn 944 with MicroMax-007 HF and VariMax HF generator) or at the Advanced Photon Source (APS) at Argonne National Laboratory (in Argonne, Illinois, USA) national synchrotron on the NECAT-24ID beamline. The diffraction data were indexed and scaled with either HKL2000. The initial structure model was built by applying molecular replacement methods with a ligand/solvent-omitted input model generated from the PDB model 3BSY. The initial models were further improved through iterative rounds of manual and automated refinement with COOT.[56] The final structure has been deposited into the Protein Data Bank PDB ID 5T2Y. Data collection and refinement statistics are presented in in the supporting information Table S3

Supplementary Material

Refer to Web version on PubMed Central for supplementary material.

Acknowledgments

We thank Dr. K. Rajashankar and the staff at NECAT-24ID (APS) for facilitating X-ray data collection for the 5T2Y structure and Dr. Alexei Soares (BNL) for the 5TYH structure, Dr. Robert Grant (MIT) and Dr. Nelson Olivier for technical assistance with protein crystallography and data processing and Dr. James Spoonamore (Broad Institute) for the MLPCN screening. We also thank Drs. Amael Madec and Cristina Zamora for their valuable assistance with the preparation of this manuscript. Financial support for this work was provided by NIH (R01-GM097241 & R03-MH096549 to BI), the Belgian American Education Foundation (fellowship to J.W.D.S.) and the Homerton College, Cambridge (Junior Research Fellowship to A.C.). Part of this work is based upon research conducted at the Northeastern Collaborative Access Team beamline 24-ID-E, which is funded by the National Institute of General Medical Sciences from the National Institutes of Health (P41 GM103403). This research used resources of the Advanced Photon Source, a U.S. Department of Energy (DOE) Office of Science User Facility operated for the DOE Office of Science by Argonne National Laboratory under Contract No. DE-AC02-06CH11357.

Abbreviations

AcCoA	acetyl coenzyme A
BOP	(Benzotriazol-1-yloxy)tris(dimethylamino)phosphonium hexafluorophosphate
DBU	1,8-Diazabicyclo[5.4.0]undec-7-ene
diNAcBac	2,4-diacetamido-2,4,6-trideoxy-α-D-glucose
PyBOP	(Benzotriazol-1-yloxy)tripyrrolidinophosphonium hexafluorophosphate
DSF	Differential scanning fluorimetry
DLS	dynamic light scattering
PLP	Pyridoxal 5′-phosphate
STD	saturation transfer difference
UndP	undecaprenyl phosphate

References

1. Silver LL. Challenges of Antibacterial Discovery. Clin Microbiol Rev. 2011; 24:71–109. [PubMed: 21233508]
2. Clatworthy AE, Pierson E, Hung DT. Targeting Virulence: A New Paradigm for Antimicrobial Therapy. Nat Chem Biol. 2007; 3:541–548. [PubMed: 17710100]
3. Baron C. Antivirulence Drugs to Target Bacterial Secretion Systems. Curr Opin Microbiol. 2010; 13:100–105. [PubMed: 20079679]
4. Barczak AK, Hung DT. Productive Steps Toward an Antimicrobial Targeting Virulence. Curr Opin Microbiol. 2009; 12:490–496. [PubMed: 19631578]
5. Cegelski L, Marshall GR, Eldridge GR, Hultgren SJ. The Biology and Future Prospects of Antivirulence Therapies. Nat Rev Micro. 2008; 6:17–27.
6. Ohtsubo K, Marth JD. Glycosylation in Cellular Mechanisms of Health and Disease. Cell. 2006; 126:855–867. [PubMed: 16959566]
7. Nothaft H, Szymanski CM. Bacterial Protein N-glycosylation: New Perspectives and Applications. J Biol Chem. 2013; 288:6912–6920. [PubMed: 23329827]
8. Aas FE, Vik Å, Vedde J, Koomey M, Egge-Jacobsen W. Neisseria gonorrhoeae O-linked Pilin Glycosylation: Functional Analyses Define Both the bBosynthetic Pathway and Glycan Structure. Mol Microbiol. 2007; 65:607–624. [PubMed: 17608667]
9. Benz I, Schmidt MA. Never Say Never Again: Protein Glycosylation in Pathogenic Bacteria. Mol Microbiol. 2002; 45:267–276. [PubMed: 12123443]
10. Szymanski CM, Wren BW. Protein Glycosylation in Bacterial Mucosal Pathogens. Nat Rev Micro. 2005; 3:225–237.
11. Vik Å, Aas FE, Anonsen JH, Bilsborough S, Schneider A, Egge-Jacobsen W, Koomey M. Broad Spectrum O-Linked Protein Glycosylation in the Human Pathogen *Neisseria gonorrhoeae*. Proc Natl Acad Sci U S A. 2009; 106:4447–4452. [PubMed: 19251655]
12. Szymanski CM, Yao R, Ewing CP, Trust TJ, Guerry P. Evidence for a System of General Protein Glycosylation in *Campylobacter jejuni*. Mol Microbiol. 1999; 32:1022–1030. [PubMed: 10361304]
13. Nothaft H, Szymanski CM. Protein Glycosylation in Bacteria: Sweeter Than Ever. Nat Rev Micro. 2010; 8:765–778.
14. Scott NE, Parker BL, Connolly AM, Paulech J, Edwards AVG, Crossett B, Falconer L, Kolarich D, Djordjevic SP, Højrup P, Packer NH, Larsen MR, Cordwell SJ. Simultaneous Glycan-Peptide Characterization Using Hydrophilic Interaction Chromatography and Parallel Fragmentation by CID, Higher Energy Collisional Dissociation, and Electron Transfer Dissociation MS Applied to the N-Linked Glycoproteome of Campylobacter jejuni. Mol Cell Proteomics. 2011; 10:M000031–MCP000201. [PubMed: 20360033]
15. Schmidt MA, Riley LW, Benz I. Sweet New World: Glycoproteins in Bacterial Pathogens. Trends Microbiol. 2003; 11:554–561. [PubMed: 14659687]
16. Sharon N. Celebrating the Golden Anniversary of the Discovery of Bacillosamine, the Diamino Sugar of a Bacillus. Glycobiology. 2007; 17:1150–1155. [PubMed: 17717023]
17. Morrison MJ, Imperiali B. The Renaissance of Bacillosamine and Its Derivatives: Pathway Characterization and Implications in Pathogenicity. Biochemistry. 2014; 53:624–638. [PubMed: 24383882]
18. Olivier NB, Chen MM, Behr JR, Imperiali B. In Vitro Biosynthesis of UDP-N,N′-Diacetylbacillosamine by Enzymes of the *Campylobacter jejuni* General Protein Glycosylation System†. Biochemistry. 2006; 45:13659–13669. [PubMed: 17087520]
19. Hartley MD, Morrison MJ, Aas FE, Børud B, Koomey M, Imperiali B. Biochemical Characterization of the O-Linked Glycosylation Pathway in *Neisseria gonorrhoeae* Responsible for Biosynthesis of Protein Glycans Containing N,N′-Diacetylbacillosamine. Biochemistry. 2011; 50:4936–4948. [PubMed: 21542610]
20. Morrison MJ, Imperiali B. Biosynthesis of UDP-N,N′-Diacetylbacillosamine in *Acinetobacter baumannii*: Biochemical Characterization and Correlation to Existing Pathways. Arch Biochem Biophys. 2013; 536:72–80. [PubMed: 23747578]

21. Kelly J, Jarrell H, Millar L, Tessier L, Fiori LM, Lau PC, Allan B, Szymanski CM. Biosynthesis of the N-Linked Glycan in *Campylobacter jejuni* and Addition onto Protein through Block Transfer. J Bacteriol. 2006; 188:2427–2434. [PubMed: 16547029]
22. Hendrixson DR, DiRita VJ. Identification of *Campylobacter jejuni* Genes Involved in Commensal Colonization of the Chick Gastrointestinal Tract. Mol Microbiol. 2004; 52:471–484. [PubMed: 15066034]
23. Szymanski CM, Burr DH, Guerry P. *Campylobacter* Protein Glycosylation Affects Host Cell Interactions. Inf Immun. 2002; 70:2242–2244.
24. Larsen JC, Szymanski C, Guerry P. N-Linked Protein Glycosylation Is Required for Full Competence in *Campylobacter jejuni* 81–176. J Bacteriol. 2004; 186:6508–6514. [PubMed: 15375132]
25. Elmi A, Watson E, Sandu P, Gundogdu O, Mills DC, Inglis NF, Manson E, Imrie L, Bajaj-Elliott M, Wren BW, Smith DG, Dorrell N. *Campylobacter jejuni* Outer Membrane Vesicles Play an Important Role in Bacterial Interactions with Human Intestinal Epithelial Cells. Infect Immun. 2012; 80:4089–4098. [PubMed: 22966047]
26. Ellis TN, Kuehn MJ. Virulence and Immunomodulatory Roles of Bacterial Outer Membrane Vesicles. Microbiol Mol Biol Rev. 2010; 74:81–94. [PubMed: 20197500]
27. Jennings MP, Jen FEC, Roddam LF, Apicella MA, Edwards JL. Neisseria gonorrhoeae Pilin Glycan Contributes to CR3 Activation During Challenge of Primary Cervical Epithelial Cells. Cell Microbiol. 2011; 13:885–896. [PubMed: 21371235]
28. Olivier NB, Imperiali B. Crystal Structure and Catalytic Mechanism of PglD from *Campylobacter jejuni*. J Biol Chem. 2008; 283:27937–27946. [PubMed: 18667421]
29. Rangarajan ES, Ruane KM, Sulea T, Watson DC, Proteau A, Leclerc S, Cygler M, Matte A, Young NM. Structure and Active Site Residues of PglD, an N-Acetyltransferase from the Bacillosamine Synthetic Pathway Required for N-Glycan Synthesis in *Campylobacter jejuni*. Biochemistry. 2008; 47:1827–1836. [PubMed: 18198901]
30. Vetting MW, LPSdC, Yu M, Hegde SS, Magnet S, Roderick SL, Blanchard JS. Structure and Functions of the GNAT Superfamily of Acetyltransferases. Arch Biochem Biophys. 2005; 433:212–226. [PubMed: 15581578]
31. Aspinall GO, McDonald AG, Pang H, Kurjanczyk LA, Penner JL. Lipopolysaccharides of *Campylobacter jejuni* Serotype O:19: Structures of Core Oligosaccharide Regions from the Serostrain and Two Bacterial Isolates from Patients with the Guillain-Barre Syndrome. Biochemistry. 1994; 33:241–249. [PubMed: 8286348]
32. Allos BM, Lippy FT, Carlsen A, Washburn RG, Blaser MJ. *Campylobacter jejuni* Strains from Patients with Guillain-Barre Syndrome. Emerg Infect Disease. 1998; 4:263–268. [PubMed: 9621196]
33. Luangtongkum T, Jeon B, Han J, Plummer P, Logue CM, Zhang Q. Antibiotic Resistance in *Campylobacter*: Emergence, Transmission and Persistence. Fut Microbiol. 2009; 4:189–200.
34. Scott DE, Coyne AG, Hudson SA, Abell C. Fragment-Based Approaches in Drug Discovery and Chemical Biology. Biochemistry. 2012; 51:4990–5003. [PubMed: 22697260]
35. Silvestre HL, Blundell TL, Abell C, Ciulli A. Integrated Biophysical Approach to Fragment Screening and Validation for Fragment-Based Lead Discovery. Proc Natl Acad Sci U S A. 2013; 110:12984–12989. [PubMed: 23872845]
36. Ellman GL. Tissue Sulfhydryl Groups. Arch Biochem Biophys. 1959; 82:70–77. [PubMed: 13650640]
37. NCBI. Inhibition of Glycoprotein Biosynthesis in Gram-Negative Pathogens Inhibitor Probe Project. https://pubchem.ncbi.nlm.nih.gov/bioassay/602402, Deposit Date: 2012–03–15
38. Friesner RA, Murphy RB, Repasky MP, Frye LL, Greenwood JR, Halgren TA, Sanschagrin PC, Mainz DT. Extra Precision Glide: Docking and Scoring Incorporating a Model of Hydrophobic Enclosure for Protein–Ligand Complexes. J Med Chem. 2006; 49:6177–6196. [PubMed: 17034125]
39. James CE, Mahendran KR, Molitor A, Bolla JM, Bessonov AN, Winterhalter M, Pagès JM. How β-Lactam Antibiotics Enter Bacteria: A Dialogue with the Porins. PLoS ONE. 2009; 4:e5453. [PubMed: 19434239]

40. Doak BC, Zheng J, Dobritzsch D, Kihlberg J. How Beyond Rule of 5 Drugs and Clinical Candidates Bind to Their Targets. J Med Chem. 2016; 59:2312–2327. [PubMed: 26457449]
41. Hann MM, Keseř GM. Finding the Sweet Spot: The Role of Nature and Nurture in Medicinal Chemistry. Nat Rev Drug Discov. 2012; 11:355–365. [PubMed: 22543468]
42. Wan ZK, Wacharasindhu S, Binnun E, Mansour T. An Efficient Direct Amination of Cyclic Amides and Cyclic Ureas. Org Lett. 2006; 8:2425–2428. [PubMed: 16706542]
43. Albe KR, Butler MH, Wright BE. Cellular Concentrations of Enzymes and their Substrates. J Theor Biol. 1990; 22143:163–195.
44. Seidler J, McGovern SL, Doman TN, Shoichet BK. Identification and Prediction of Promiscuous Aggregating Inhibitors among Known Drugs. J Med Chem. 2003; 46:4477–4486. [PubMed: 14521410]
45. Pantoliano MW, Petrella EC, Kwasnoski JD, Lobanov VS, Myslik J, Graf E, Carver T, Asel E, Springer BA, Lane P, Salemme FR. High-Density Miniaturized Thermal Shift Assays as a General Strategy for Drug Discovery. J Biomol Screen. 2001; 6:429–440. [PubMed: 11788061]
46. Wallace AC, Laskowski RA, Thornton JM. LIGPLOT: a program to generate schematic diagrams of protein-ligand interactions. Protein Eng. 1995; 8:127–134. [PubMed: 7630882]
47. Dunford JE, Kwaasi AA, Rogers MJ, Barnett BL, Ebetino FH, Russell RGG, Oppermann U, Kavanagh KL. Structure–Activity Relationships Among the Nitrogen Containing Bisphosphonates in Clinical Use and Other Analogues: Time-Dependent Inhibition of Human Farnesyl Pyrophosphate Synthase. J Med Chem. 2008; 51:2187–2195. [PubMed: 18327899]
48. Morrison MJ, Imperiali B. Biochemical Analysis and Structure Determination of Bacterial Acetyltransferases Responsible for the Biosynthesis of UDP-N,N′-Diacetylbacillosamine. J Biol Chem. 2013; 288:32248–32260. [PubMed: 24064219]
49. Lertpiriyapong K, Gamazon ER, Feng Y, Park DS, Pang J, Botka G, Graffam ME, Ge Z, Fox JG. *Campylobacter jejuni* Type VI Secretion System: Roles in Adaptation to Deoxycholic Acid, Host Cell Adherence, Invasion, and in vivo Colonization. PLoS ONE. 2012; 7:e42842. [PubMed: 22952616]
50. Isabella, Vincent M., Campbell, Arthur J., Manchester, J., Sylvester, M., Nayar, Asha S., Ferguson, Keith E., Tommasi, R., Miller, Alita A. Toward the Rational Design of Carbapenem Uptake in *Pseudomonas aeruginosa*. Chem Biol. 2015; 22:535–547. [PubMed: 25910245]
51. Lo AWH, Van de Water K, Gane PJ, Chan AWE, Steadman D, Stevens K, Selwood DL, Waksman G, Remaut H. Suppression of Type 1 Pilus Assembly in Uropathogenic *Escherichia coli* by Chemical Inhibition of Subunit Polymerization. J Antimicrob Chemother. 2014; 69:1017–1026. [PubMed: 24324225]
52. Adams LA, Sharma P, Mohanty B, Ilyichova OV, Mulcair MD, Williams ML, Gleeson EC, Totsika M, Doak BC, Caria S, Rimmer K, Horne J, Shouldice SR, Vazirani M, Headey SJ, Plumb BR, Martin JL, Heras B, Simpson JS, Scanlon MJ. Application of Fragment-Based Screening to the Design of Inhibitors of *Escherichia coli* DsbA. Angew Chem Int Ed Engl. 2015; 54:2179–2184. [PubMed: 25556635]
53. Moore JD, Rossi FM, Welsh MA, Nyffeler KE, Blackwell HE. A Comparative Analysis of Synthetic Quorum Sensing Modulators in *Pseudomonas aeruginosa*: New Insights into Mechanism, Active Efflux Susceptibility, Phenotypic Response, and Next-Generation Ligand Design. J Am Chem Soc. 2015; 137:14626–14639. [PubMed: 26491787]
54. Ménard R, Schoenhofen IC, Tao L, Aubry A, Bouchard P, Reid CW, Lachance P, Twine SM, Fulton KM, Cui Q, Hogues H, Purisima EO, Sulea T, Logan SM. Small-Molecule Inhibitors of the Pseudaminic Acid Biosynthetic Pathway: Targeting Motility as a Key Bacterial Virulence Factor. Antimicrob Agents Chemother. 2014; 58:7430–7440. [PubMed: 25267679]
55. Curtis MM, Russell R, Moreira CG, Adebesin AM, Wang C, Williams NS, Taussig R, Stewart D, Zimmern P, Lu B, Prasad RN, Zhu C, Rasko DA, Huntley JF, Falck JR, Sperandio V. QseC Inhibitors as an Antivirulence Approach for Gram-Negative Pathogens. mBio. 2014; 5:e02165. [PubMed: 25389178]
56. Emsley P, Cowtan K. Coot: Model-Building Tools for Molecular Graphics. Acta Cryst Sect D. 2004; 60:2126–2132. [PubMed: 15572765]

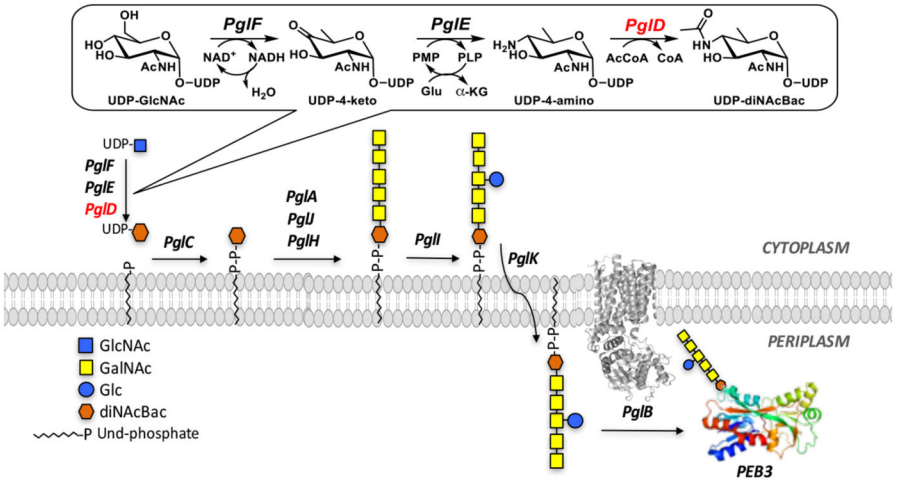

Figure 1.

Schematic representation of the *C. jejuni* N-linked protein glycosylation pathway. Enzymes are shown in italics with the oligosaccharyl transferase PglB shown as determined in PDB 3RCE. Also shown is an N-linked glycosylation substrate PEB3 (PDB: 2HXW), which is a virulence factor in periplasm that is modified by N-linked glycosylation. Inset highlights the three sugar-modifying enzymes that convert UDP-GlcNAc to UDP-diNAcBac.

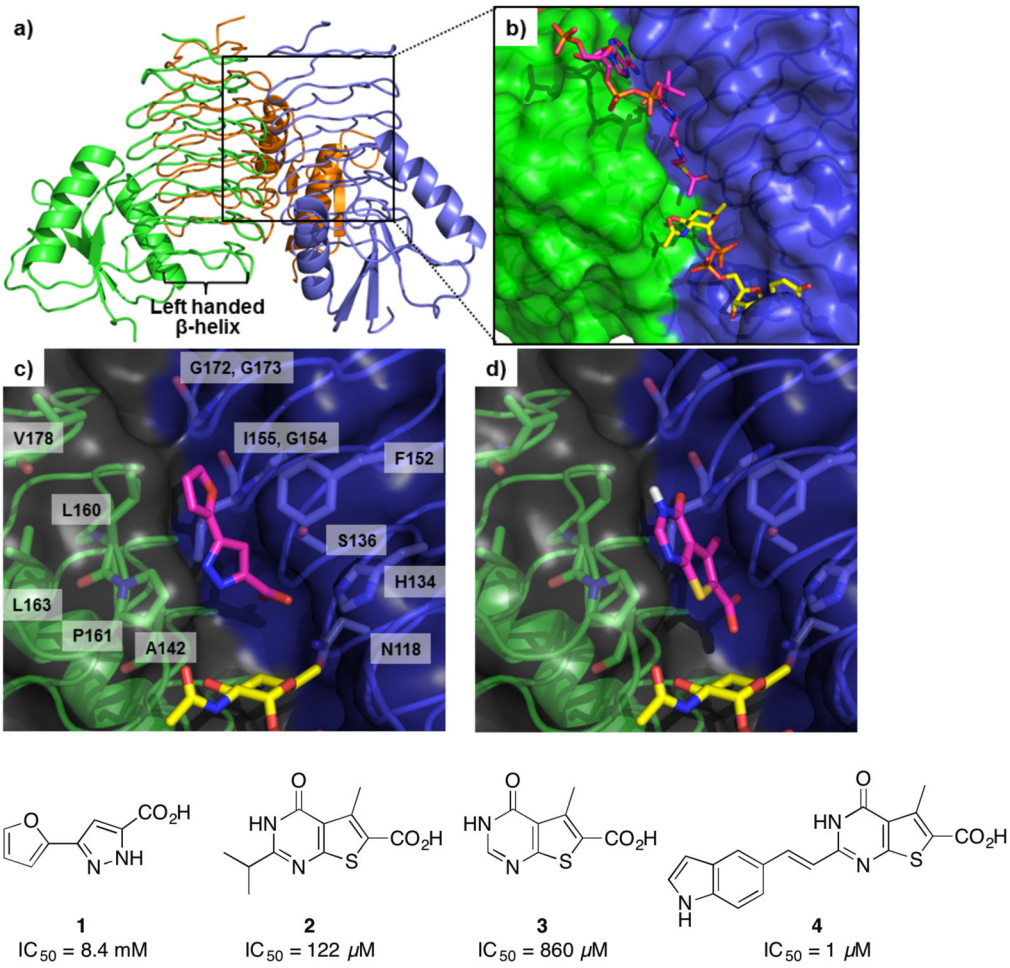

Figure 2.

Structure analysis of *C. jejuni* PglD. (a) Crystal structure of the PglD homotrimer (PDB 3BSY) in cartoon representation; individual protomers are colored in green, blue and orange. (b) Expanded of view of the PglD active site protein surface with the AcCoA substrate shown in stick representation (magenta, PDB 3BSY) as well as the UDP-4-amino-sugar substrate (yellow, PDB 3BSS). (c) Crystal structure of fragment **1** (magenta) bound to PglD with a semi-transparent surface and selected side-chain residues shown in stick representation and annotated (PDB 5TYH). (d) Docking output pose generated for compound **3** (Glide, Maestro).[38]

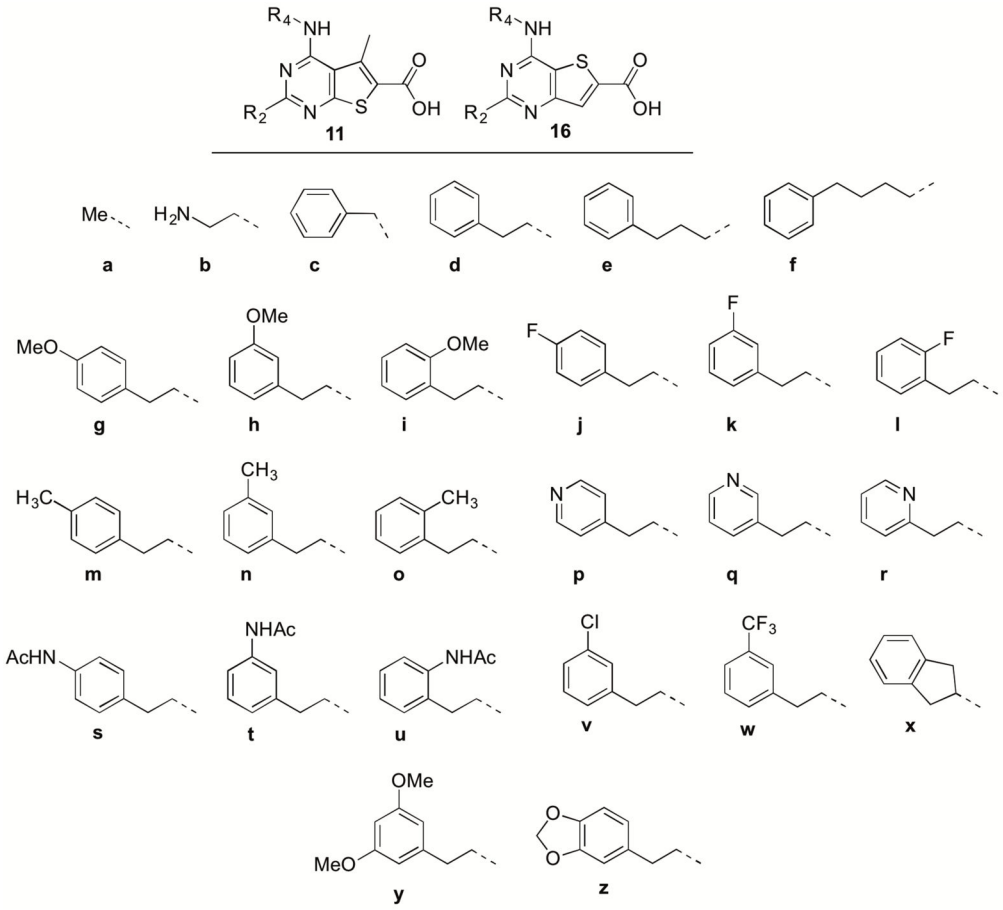

Figure 3.

Representative examples of thienopyrimidine-6-carboxylate inhibitors of *C. jejuni* PglD; Core **11**: R_2 = **a – z**; R_4 = **a – z**; Core **16:** R_2 = **d**, **h**; R_4 = **a**.

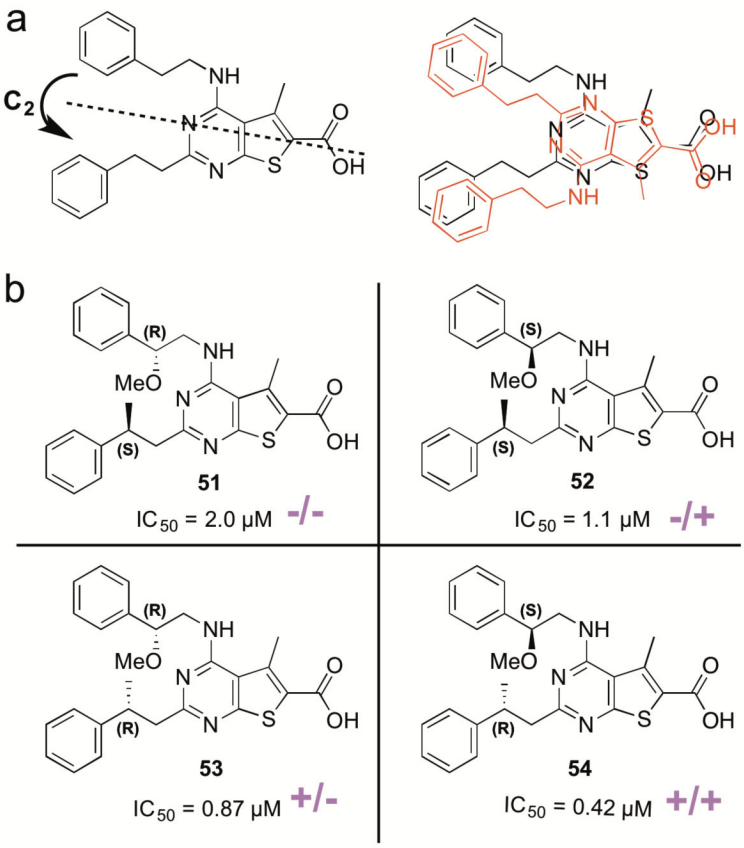

Figure 4.

(**a**) Illustration of the quasi C_2 symmetry axis of the disubstituted inhibitors (**b**) SAR of inhibitors **51** – **54** with rigidified R_2 and R_4 substituents; magenta symbols represent stereochemical preference of R_2 and R_4 substituents with respect to the PglD protein surface and highlight the mismatched/matched pattern.

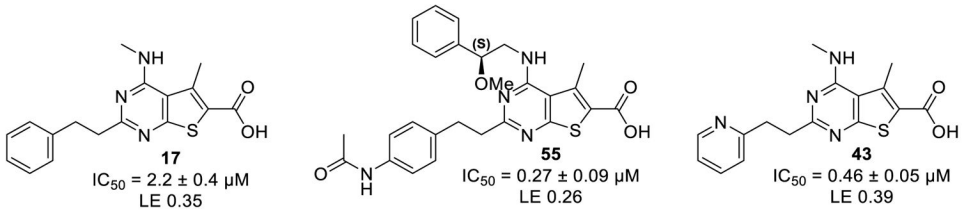

Figure 5.
Structures of key inhibitors discussed in this section: **17**, **43** and **55**.

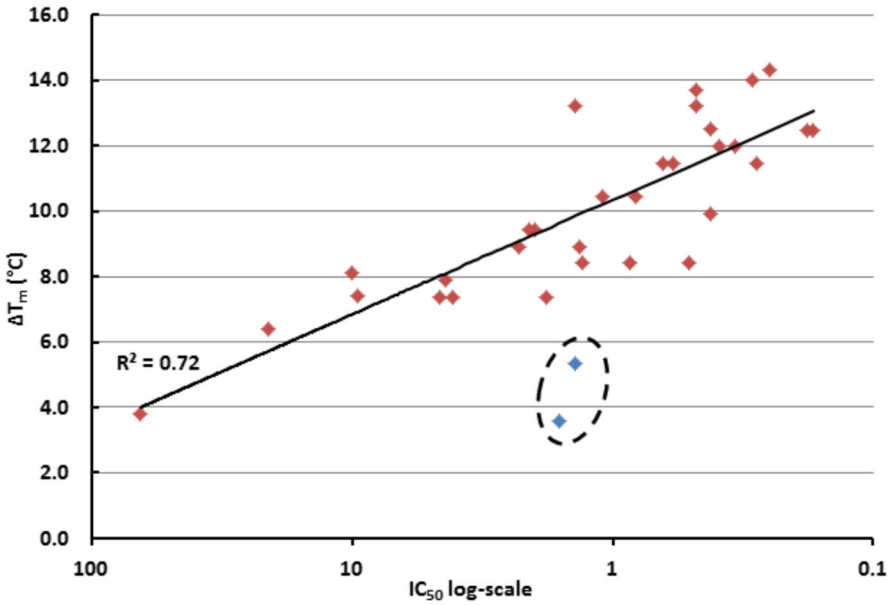

Figure 6.

Correlation between the *in vitro* potency against PglD and the T_m (calculated from the first derivative of the thermal melting curve) of the PglD/inhibitor complexes with core **11**; thermal melt assays were performed with 10 μM PglD and 100 μM compound. Correlation coefficient provided for all data indicated by red diamond. Inhibitors with R_4 = **b** (ethylamine) (blue diamond, circled) appear as outliers and are omitted from the calculation of the correlation coefficient.

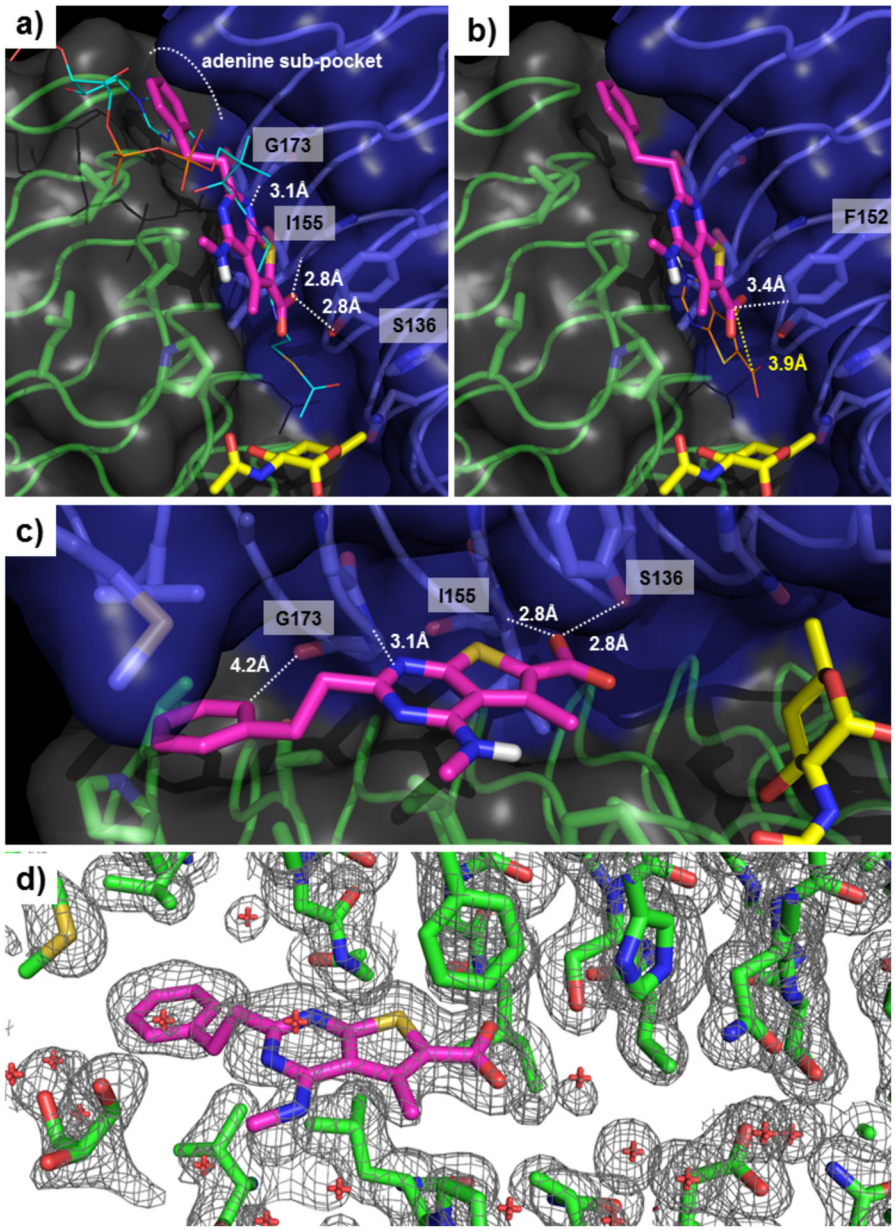

Figure 7.

Co-crystal structure of the PglD/**17** complex (PDB 5T2Y). (**a**) Inhibitor **17** shown in sticks presentation (magenta) and overlayed with AcCoA substrate in lines (cyan, PDB 3BSY) and sugar substrate in sticks (yellow, PDB 3BSS). (**b**) overlay with the computational docking pose of compound **2** in line representation (orange). (**c**) Side-view highlighting the AcCoA adenine sub-pocket and interaction between **17** and residues Gly173, Ile155 and Ser136. White dashed lines indicate distances between **17** and PglD side-chain residues; yellow dashed line shows distance between the carboxylate computational docking pose and crystal structure. (**d**) Composite omit map $2F_o - F_c$ contoured at 1.0 σ generated with the built in functionality of the PHENIX software and image generated in PYMOL.

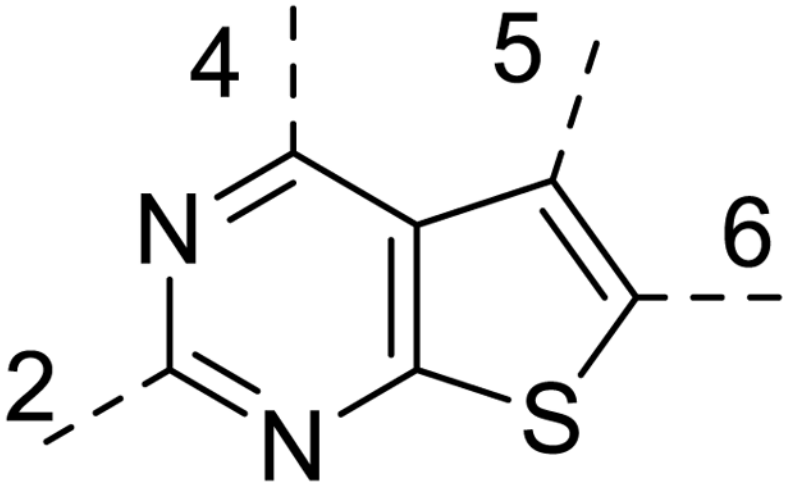

Scheme 1.
General structure and numbering system of the thienopyrimidine core.

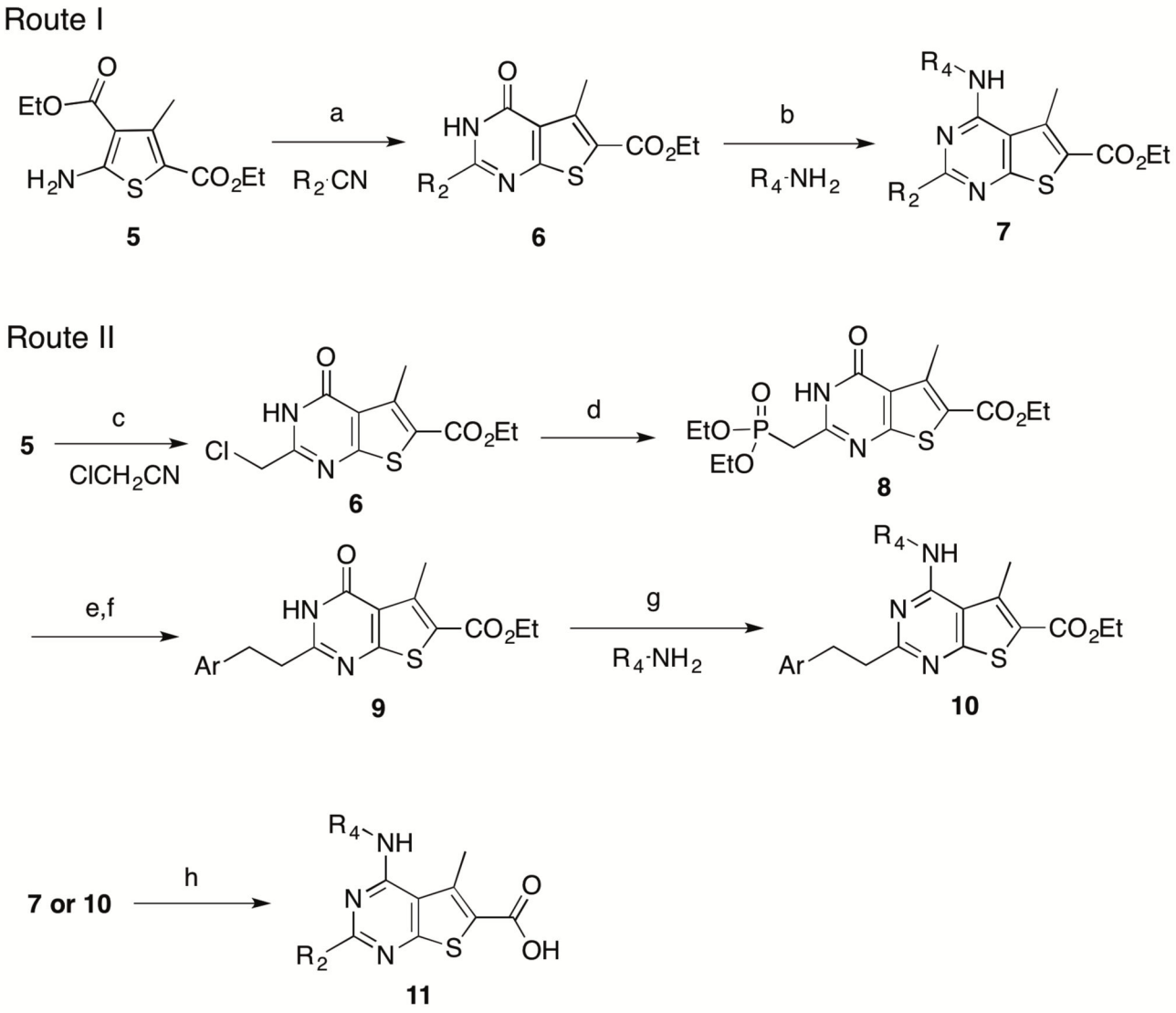

Scheme 2.

Synthesis of inhibitors with thienopyrimidine-6-carboxylate core **11**

Conditions: (a) 1.2 equiv. R_2CN, 4 M HCl in 1,4-dioxane, 90°C (50–90%); (b) 1.5 equiv. R_4NH_2, 1.3 equiv. PyBOP, 3 equiv. DBU, MeCN, RT (40–90%); (c) 1.2 equiv. $ClCH_2CN$, 4 M HCl in 1,4-dioxane, 90°C (50–90%) (d) 20 equiv. $P(OEt)_3$, 145°C (85%); (e) 1.5 equiv. NaH, 2 equiv. ArCHO, THF, RT (70–90%); (f) 10% $Pd(OH)_2/C$, THF/MeOH 1:1, 60°C (quant.); (g) 1.5 equiv. R_4NH_2, 1.3 equiv. PyBOP, 3 equiv. DBU, MeCN, RT (40–90%) (h) 3 equiv. NaOH, THF/MeOH/H_2O 2:1:1, RT (50–80%).

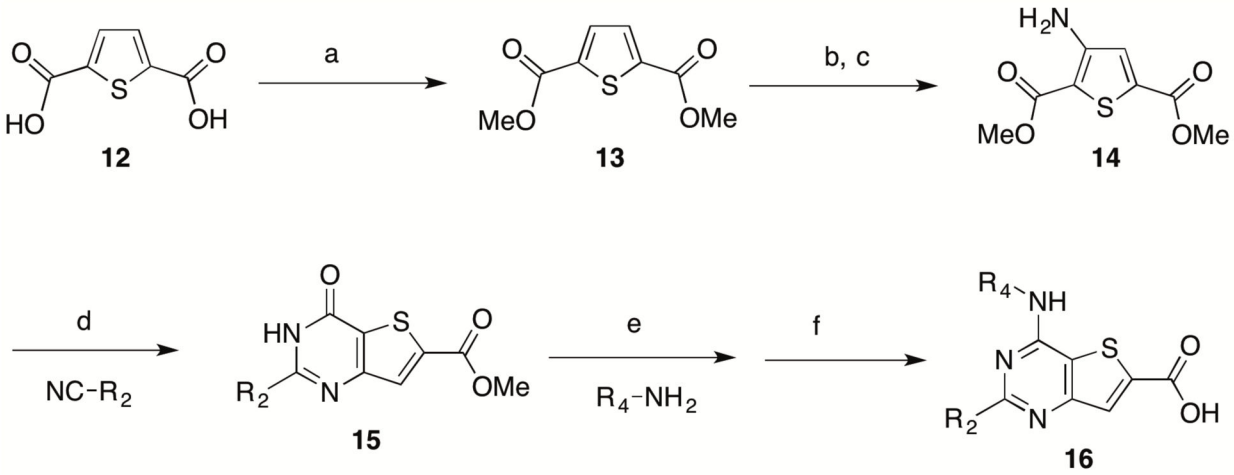

Scheme 3.

Synthesis of inhibitors with thienopyrimidine-6-carboxylate core **16**

Conditions: (a) 4 equiv. $SOCl_2$, MeOH, 50°C (99%); (b) 2 equiv. HNO_3, H_2SO_4, RT; (c) 10% $Pd(OH)_2/C$, THF/MeOH 1:1, RT (93% over 2 steps); (d) 1.2 equiv. R_2CN, 4 M HCl in 1,4-dioxane, 90°C (60–80%); (e) 1.5 equiv. R_4NH_2, 1.3 equiv. PyBOP, 3 equiv. DBU, MeCN, RT (40–90%); (f) 3 equiv. NaOH in THF/MeOH/H_2O 2:1:1, RT (50–80%).

Table 1

Experimental data obtained for selected inhibitors (Figures 3 and 4): IC_{50} values determined with the continuous *C. jejuni* PglD inhibition assay, calculated ligand efficiency (LE), thermal stabilization of the PglD/ligand complex with the DSF assay, and cLogP values calculated with built-in functionality of the ChemDraw® commercial software package. Compounds **51**–**54** (Figure 4): 2MPE: 2-methoxy-2-phenylethyl and 2PP: 2-phenylpropyl.

Compound #	Scaffold	R_2	R_4	IC_{50}/(μM)	LE	ΔT_m/(°C)	cLogP
17	**11**	**d**	**a**	2.2 ± 0.4	0.35	7.4	4.44
18	**11**	**d**	**b**	1.6	0.32	3.6	1.48
19	**11**	**d**	**c**	4.5	0.26	*nd*	5.89
20	**11**	**d**	**d**	1.4	0.27	13.2	6.54
21	**11**	**d**	**g**	0.54	0.27	*nd*	6.46
22	**11**	**d**	**h**	0.45	0.28	*nd*	6.46
23	**11**	**d**	**i**	0.48	0.28	13.7	6.46
24	**11**	**d**	**j**	0.42	0.29	*nd*	6.68
25	**11**	**d**	**k**	0.39	0.29	*nd*	6.68
26	**11**	**d**	**l**	0.48	0.29	13.2	6.68
27	**11**	**d**	**m**	0.72	0.28	*nd*	6.99
28	**11**	**d**	**n**	0.42	0.29	*nd*	6.99
29	**11**	**d**	**o**	0.25	0.30	14.3	6.99
30	**11**	**d**	**p**	0.39	0.30	12.0	5.04
31	**11**	**d**	**q**	0.34	0.30	12.0	5.04
32	**11**	**d**	**r**	0.42	0.30	12.5	5.04
33	**11**	**s**	**a**	2.4	0.29	*nd*	3.46
34	**11**	**t**	**a**	3.5	0.28	*nd*	3.46
35	**11**	**u**	**a**	9.0	0.26	*nd*	3.46
36	**11**	**d**	**x**	1.0	0.27	*nd*	6.42
37	**11**	**d**	**y**	0.37	0.26	*nd*	6.55
38	**11**	**d**	**z**	0.59	0.26	11.5	6.50
39	**11**	**e**	**a**	4.4	0.31	7.9	4.97

Compound #	Scaffold	R_2	R_4	IC_{50}/(μM)	LE	ΔT_m/(°C)	cLogP
40	**11**	**f**	**a**	4.1	0.30	7.4	5.50
41	**11**	**h**	**a**	1.1 ± 0.2	0.33	8.4	4.36
42	**11**	**k**	**a**	2.3	0.33	8.9	4.58
43	**11**	**q**	**a**	0.46 ± 0.05	0.39	8.4	2.94
44	**11**	**s**	**b**	1.4	0.28	5.3	0.50
45	**11**	**s**	**r**	0.28	0.27	11.5	4.06
46	**11**	**v**	**a**	2.1	0.33	9.4	5.15
47	**11**	**w**	**a**	4.6	0.28	7.4	5.32
48	**11**	**z**	**a**	1.8	0.31	7.4	4.41
49	**16**	**d**	**a**	3.9	0.34	4.8	4.45
50	**16**	**h**	**a**	1.4	0.34	5.9	4.37
51	**11**	2PP(S)	2MPE(R)	2.0	0.24	9.4	6.50
52	**11**	2PP(S)	2MPE(S)	1.1	0.25	10.4	6.50
53	**11**	2PP(R)	2MPE(R)	0.87	0.27	*nd*	6.50
54	**11**	2PP(R)	2MPE(S)	0.42	0.27	9.9	6.50
55	**11**	**s**	2MPE(S)	0.27 ± 0.09	0.26	12.5	5.12